4-7-1997

Preparation and characterization of bulk nanostructures Cu-Co magnetic alloys

Michael Gartley

PREPARATION AND CHARACTERIZATION OF BULK NANOSTRUCTURED Cu-Co MAGNETIC ALLOYS

Michael G. Gartley[1]
Center for Materials Science and Engineering
Rochester Institute of Technology

A thesis submitted in partial fulfilment
of the requirments for the
Master of Science in
Materials Science and Engineering

Approved by:

Vinnie Gupta (Advisor)	*Alan Entenberg*
Linda Meichle	*Marietta Scanlon*

Peter Cardegna (Program Director)

[1] email: mgg3357@rit.edu homephone: 716/ 426-7178

April 7, 1997

I, **Michael G. Gartley**, grant permission to Wallace Memorial Library of Rochester Institute of Technology to reproduce my thesis, "The preparation and characterization of bulk nanostructured Cu-Co magnetic alloys", in part or in whole. Any reproduction will not be for commercial use or profit.

michael g. gartley

Table of Contents

Abstract

With new fabrication and measurement technologies now readily available, much attention has been focused on nanostructured materials. The sub-micron scale features of these materials gives them unique physical properties. To understand these properties, conventional methods of materials characterization are not always applicable. Therefore, new methods of characterization are needed for these nanostructured materials.

In this project, we have developed nanostructured Cu-Co alloys. Alloys contain 0.3-5.0 wt% cobalt. Alloys are solution-annealed such that the cobalt dissolves in the solid copper phase. By subsequently aging the solid solutions with 1.5% Co at lower temperatures, the cobalt precipitates out of solution and forms precipitate particles with sizes ranging from 0-300A. The growth rate of these particles is a function of the aging temperature. These sub-micron sized cobalt particles possess interesting and useful magnetic properties.

It was found that the Cu-Co solid solutions behave paramagnetically, with their initial susceptibility being proportional to the square of the cobalt content. For the aged alloys, magnetic methods are used to characterize the material. Using vibrating sample magnetometry, we measured saturation magnetization and coercivity. The saturation magnetization is a function of amount of cobalt that has precipitated out of solid

solution. Cobalt concentration in solid solution was also obtained from x-ray diffraction analysis. The coercivity is a function of cobalt particle size and shape distribution. These magnetic particles were also characterized by magnetic force microscopy.

Acknowledgments

First I would like to acknowledge my thesis advisor, Vinnie Gupta. Not only for the patience and support in starting my own project from the ground up, but for making this project a meaningful experience in all respects. Thanks for the long hours of your own time and your creative perspective.

I would also like to acknowledge the support of many people in the physics department. Thanks to Alan Entenberg and Linda Meichle for use of their lab and getting me started in working with magnetic materials. Linda Meichle was indispensable for her help in the interpretation of the VSM results and for stimulating discussions. Thanks to Bill VanDerveer for technical support. Thanks to Peter Cardegna for financial support and use of his equipment. I would also like to thank Mike Jackson of the Microelectronic Engineering department for helping with SEM work. Thanks to Marietta Scanlon for helpful comments and sense of humor.

I would like to acknowledge the technical assistance of everyone in the machine shop, including Tom Locke, Dave Hathaway, and Jim Grenier. They always went far out of their way to assist me.

Thanks to people in the industry for their interest in my project. In particular, Ron Ziolo at Xerox Corporation for insightful discussions and TEM work. Thanks to the

people at Hoosier magnetics for supplying grinding materials during a phase (since been abandoned) when I was trying to grind cobalt powders.

Last but far from least, I would like to thank my family. Thanks for the understanding and unconditional support. My fiance, Karen, was always glad to hear about my problems and successes and put up with crazy hours of work. She helped keep me sane and happy.

Summary of variables used

α	growth rate coefficient
a	lattice parameter
a_o	precise lattice parameter
b	constant related to x-ray peak breadth
c	cobalt concentration
c_s	solubility of cobalt in copper
d	cobalt particle size
d_p	critical size for superparamagnetic behavior
d_s	critical size for single-domain behavior
D_o	diffusion constant
$D_{Cu\text{-}Co}$	diffusion coefficient of cobalt in copper
γ	rate constant
I	x-ray intensity
I_o	background x-ray signal
k	constant
λ	x-ray wavelength
t	time
θ	x-ray collection angle
T	temperature
y	x-ray spectrum peak location

Index of figures and tables

Chapter 1

Chapter 2

Chapter 3

Chapter 4

Chapter 5

Chapter 1. Introduction

1.1. Project motivation and goals

Recently, much attention has been focused on so-called "nanostructured" materials. These materials have microstructures which are developed on the **nano**meter (10^{-9} m) scale. Such materials have unique and useful properties. Nanostructured materials have recently found many applications in the digital storage and semiconductor industries.

In this project a binary alloy system will be developed in which one can precipitate and grow nanometer sized particles. The solid nanometer sized particles will be imbedded in another solid phase. The alloy will be prepared in the bulk form to promote isotropic behavior and eliminate surface effects.

The copper-cobalt binary alloy system was chosen for this project. One feature of this materials system that makes it novel is the lack of intermediate phases and the negligible room temperature solubility of cobalt in copper. However, at elevated temperatures the solubility of cobalt in copper exceeds 4 wt%. Another important feature of copper-cobalt alloys is that cobalt is inherently magnetic, whereas copper is weakly diamagnetic. This allows the use of magnetic measurement methods for characterizing the alloy.

The "classic" precipitation hardening procedure will be used to grow nanometer sized cobalt particles in a solid copper phase. The first step in this process is to solution-anneal the alloy above its solvus temperature. After the alloy reaches an equilibrium state, there should exist a single phase solid solution of cobalt in copper.

The solvus temperature for this binary system depends on its composition. This dependence is represented by the solvus curve, shown in the Cu-Co phase diagram (Figure 1.1). By heating an alloy above its solvus temperature, we can create a single phase solid solution material.

Once cobalt is in solid solution, the alloy is quenched to "freeze" in this state. The resulting material is a supersaturated metastable solid solution at room temperature. If the material is slowly cooled to room temperature, the amount of cobalt in solution is described by the solvus at room temperature. Which, in the case of this materials system, is negligible.

The supersaturated metastable solid solution can be aged at a temperature which is below the solvus curve in the phase diagram. This aging precipitates some cobalt out of solid solution. The actual amount of cobalt that precipitates depends on the aging time and temperature. Some of the cobalt atoms that are driven out of solution form nuclei to which other cobalt atoms attach. It is at these nuclei that cobalt precipitates grow.

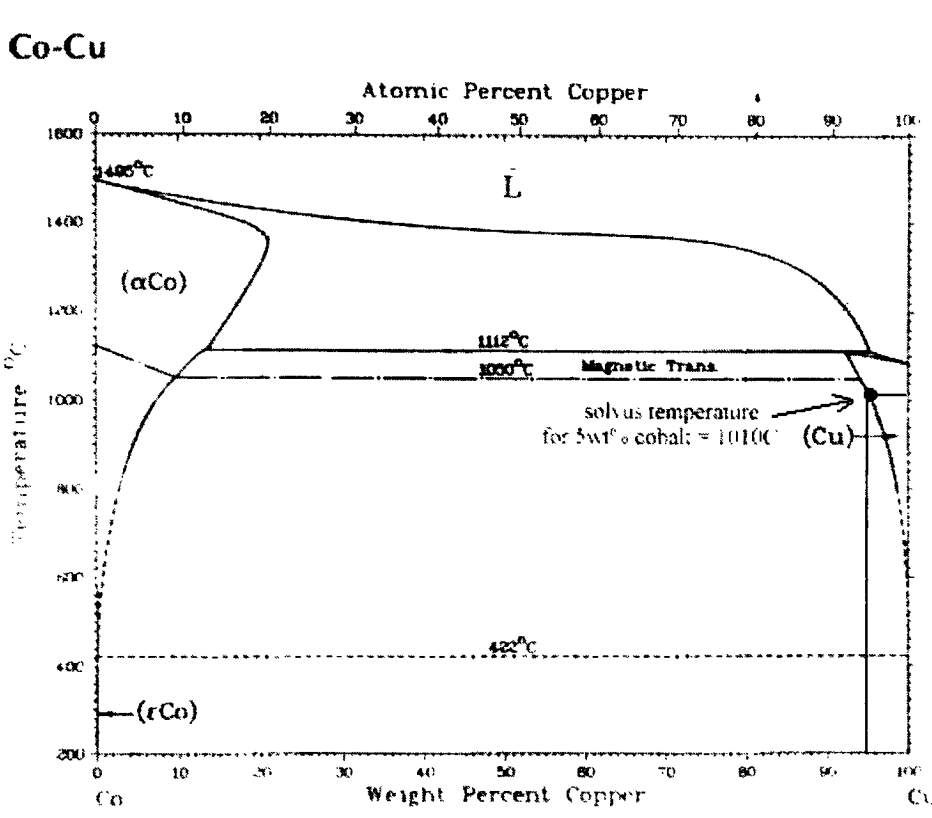

Figure 1.1. Cu-Co binary phase diagram[1].

The growth kinetics of the precipitates are controlled by the aging time and temperature. At higher temperatures, the growth is faster due to a larger diffusion coefficient. The diffusion coefficient is a measure of how quickly the cobalt atoms can diffuse in the solid copper phase. At higher temperatures, cobalt has a higher solid solubility which limits the amount of cobalt available for particle growth. Therefore, one can control the cobalt particle size distribution by selecting appropriate heat-treatments. Higher temperatures promote a faster growth rate. Longer aging times yield larger cobalt particles.

[1] ASM Metals handbook, Volume 3: Alloy Phase Diagrams, ASM International, 1991.

1.2. Project overview

In order to successfully develop our materials system, we must carefully choose the material composition. In addition, the heat treatment parameters must also be chosen with care.

A composition of 1.5% cobalt balanced by copper ($Cu_{98.5}Co_{1.5}$) will be used for most of the studies. This composition is well inside the solvus line on the phase diagram and should create a fairly dilute dispersion of cobalt particles.

The temperature at which we will solution-anneal the materials will be 1020°C. This temperature is high enough to quickly attain an equilibrium solid solution single phase. The solution-anneal temperature is also safely below the liquidus line, which reduces the chance of accidentally melting the sample.

For the aging process, we pick two temperatures, 700°C and 750°C. These temperatures are far enough apart to see a significant difference in the growth rate of precipitate particles. The two temperatures are also low enough such that we can age between 0 and 250 minutes and still have nanometer sized cobalt particles. These temperatures are also high enough such that cobalt in excess of solubility limit, will be completely precipitated out of solution after a few minutes.

In order to detect how much cobalt is **in** solid solution at any stage in the process, we will use X-ray diffraction (XRD). XRD analysis provides the lattice parameter of the copper-cobalt solid solution. The lattice parameter of the alloy is a function of the amount of cobalt in solid solution.

A method for indirectly measuring the amount of cobalt that is **out** of solid solution is Vibrating Sample Magnetometry (VSM)[2]. VSM analysis yields the saturation magnetization of the material. The saturation magnetization of a magnetic material is directly proportional to the amount of ferromagnetic phase. Knowing the total mass of the material, one can easily find the wt% cobalt that has precipitated out of solution.

In order to determine the size of the precipitates, we will use magnetic force microscopy[3] (MFM). MFM analysis allows one to image the magnetic fields above the cobalt particles on a nanometer-sized scale. This small scale is necessary because the cobalt particles themselves will be nanometer sized. These magnetic fields indicate many things about the cobalt particles including size, shape, magnetic state, and the orientation of the magnetization vector.

Lastly, VSM will be used to qualitatively describe the size of the cobalt particles. The VSM can measure coercivity, which is an intrinsic property of ferromagnetic materials.

---

[2] S. Foner, Versatile and sensitive Vibrating Sample Magnetometer, Rev. Sci. Instr., **40** (7), 1959.
[3] D. Rugar et al, Magnetic force microscopy: General principles and application to longitudinal recording media, J. Appl. Phys.,**68** (3), p1169, 1990.

We will exploit the fact that the coercivity of small magnetic particles is well understood and found to depend on their size.

1.3. Literature survey: materials aspects

The primary mechanism for cobalt precipitation and particle growth is diffusion. Dohl, Macht and Naundorf[4] have measured the diffusion coefficient of cobalt atoms in solid copper. It was found that the diffusion coefficient is given by

$$D_{Co \to Cu} = 0.43 e^{-2.22 eV/kT} \qquad (1.1)$$

in cm^2/s. To show how the diffusion coefficient changes by orders of magnitude at different temperatures, we show its value at various temperatures in Table 1.1

T (C)	D_{Co-Cu} (cm^2/s)
30	5.25E-38
700	1.37E-12
750	5.01E-12
800	1.62E-11
900	1.25E-10
1020	9.62E-10

Table 1.1. Values of the diffusion coefficient of cobalt in copper at various temperatures.

Notice that the diffusion coefficient at the solution-treatment temperature (1020°C) is 3 orders of magnitude larger that at the aging temperatures (700-750°C) and 28 orders of magnitude larger than at the room temperature.

[4] R. Dohl et al, Measurement of the diffusion coefficient of cobalt in copper, Phys. Stat. Sol. A, **86**, p603, 1984.

Although the copper-cobalt phase diagram describes the solubility of cobalt in copper, a more accurate description is needed. Servi and Turnbull[5] have shown that the solvus line is described by

$$\log c_s = 2.853 - 2.875 \cdot \frac{1000}{T} \tag{1.2}$$

where c_s is the solvus concentration and T is the absolute temperature in kelvin.

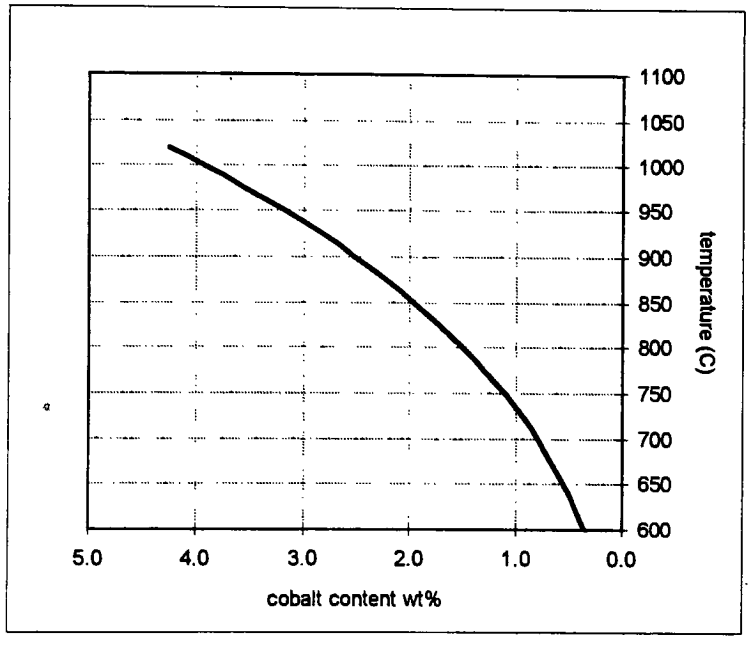

Figure 1.2. Solvus curve calculated using the method of Servi and Turnbull.

This equation is best understood when graphically presented in Figure 1.2. One can see that the solubility of cobalt in copper quickly approaches zero as the temperature decreases. Since we are interested in the precise values of this solubility at various temperatures, we list them in Table 1.2.

[5] I. S. Servi, D. Turnbull, Thermodynamics and kinetics of precipitation in the Copper-Cobalt system. Acta. Meta., **14**, p161, 1966.

T (C)	c_s (% Co)
30	0.000
700	0.791
750	1.103
800	1.491
900	2.524
1020	4.261

Table 1.2. Values of the solubility of cobalt in copper at various temperatures.

The precipitation of cobalt particles out of a solid solution in copper has been studied extensively. In 1957, J. J. Becker[6] was the first to use magnetic measurements to determine the sizes of the cobalt precipitates.

In his first paper, he discovered that precipitation hardened $Cu_{98}Co_2$ alloys behaved superparamagnetically. Superparamagnetic materials have the same magnetic properties as normal paramagnets, except that they are easily saturated in moderate magnetic fields. From the magnetization data, Becker developed a method for calculating an "effective" particle size. He also determined how much cobalt was precipitated out of solution using the saturation magnetization of the material. The saturation magnetization is the magnetization of the material when all magnetic moments are aligned.

Two subsequent papers resulted from this initial study. First[7], he studied the effect of a magnetic field during the heat treatments on the magnetic properties. He then[8] used

[6] J. J. Becker, Magnetic method for the measurement of precipitate particle sizes in a Cu-Co alloy, Trans. AIME, p59, Jan 1957.
[7] J. J. Becker, Precipitation and magnetic annealing in a Cu-Co alloy, Trans. AIME, p139, Feb 1958.

his method for determining precipitate particle size to understand the tensile and mechanical properties of the alloys.

J. J. Becker's method has been used to understand the influence of doping on the precipitation process. Breu, Gust and Predel[9] determined that the addition of 0.3% Ge slows the precipitation process down considerably. Although they include a TEM picture, they do not attempt to explain the picture or use other methods to validate their results.

1.4. Literature survey: magnetic properties of cobalt and copper-cobalt alloys

The magnetic properties of copper-cobalt solid solutions have been studied by Tournier and Blandin[10]. It was found that copper-cobalt solid solutions behave paramagnetically. It was also determined that the initial susceptibility, X_o, of the alloys depends on the cobalt content,

$$X_o = aC^2 \qquad (1.3)$$

where a is a constant and C is the cobalt content.

---

[8] J. J. Becker, J. D. Livingston, A study of precipitation-hardening employing magnetic measurements, Trans. AIME, p316, June 1958.

[9] M. Breu, W. Gust, B. Predel, Influence of doping on the early stages of precipitation in Cu-Co-base alloys, Mat. Sci. Eng., **A151**, p61, 1992.

[10] R. Tournier, A. Blandin, Influence of interactions between impurities on the appearance of magnetic moments in copper-cobalt dilute alloys, Phys. Rev. Lett., **24** (8), p397, 1970.

Childress and Chien[11] developed thin film materials with cobalt particles dispersed in a solid copper matrix. They were able to sputter a solid solution of cobalt in copper. Subsequent heat treatments were done to precipitate the cobalt out of solution. They report on the influence of sputtering and heat treatment parameters on the magnetic properties of the films. However, they give no indication of the actual sizes of the cobalt particles in each film.

Some researchers have attempted to understand how size affects the magnetic properties of individual cobalt particles. Gangopadhyay and Hadjipanayis[12] were able to synthesize cobalt particles 50-350A in size. This was done by evaporation deposition onto a glass substrate. They found a maximum coercivity of 1600 Oe for an assembly of 350A particles at room temperature. This result does not reflect the coercivity of an individual cobalt particle for a few reasons. First, they determined that their particles had an appreciable oxide coating, which tends to raise the coercivity of the material. They also do not consider particle-particle interactions of their film. A TEM picture shows close packing of the particles which would result in higher coercivities.

An interesting phenomena which exists in these nanostructured copper-cobalt alloys is known as giant magnetoresistance (GMR). A magnetoresistive material shows an

[11] J. R. Childress, C. L. Chien, Reentrant magntic behavior in fcc Cu-Co alloys, Phys. Rev. B, **43** (10), p8089, 1991.
[12] S. Gangopadhyay et al, Magnetic properties of ultrafine Co particles, IEEE Trans. Mag., **28** (5), p3174, 1992.

appreciable change in electrical resistivity when a magnetic field is applied. The magnetoresistive effect in some copper-cobalt alloys is considered to be "giant" because resistivity changes by more than 40%. Magnetoresistive materials have recently been paid much attention in the literature[13,14,15] because of their potential applications in the magnetic recording industry.

1.5. Literature survey: new methods for synthesis of copper-cobalt alloys

Most people working with copper-cobalt alloys prepare their materials in the form of thin films or the bulk. However, recently some researchers have devised alternate preparation methods.

Some researchers have found that nanometer sized copper and cobalt particles can be chemically precipitated out of solution. Chow et al[16] report on a process referred to as the "polyol process." They have been able to precipitate face centered cubic (fcc) cobalt particles out of solution at 190°C, even though cobalt is normally hexagonal close packed (hcp) below 400°C. The reason for the formation of a fcc cobalt phase is that it requires much less energy to nucleate it on fcc copper sites.

---

[13] R. H. Yu et al, Magnetic properties and giant magnetoresistance in magnetic granular Co_xCu_{100-x} alloys, J. Phys. D: Appl. Phys. **28**, p1770, 1995.
[14] J. Q. Xiao, J. S. Jiang, C. L. Chien, Giant magnetoresistance in nonmultilayer magnetic systems, Phys. Rev. Lett., **68** (25), p3749, 1992.
[15] A. E. Berkowitz et al, Giant magnetoresistance in heterogeneous Cu-Co alloys, Phys. Rev. Lett., **68** (25), p3745, 1992.
[16] G. M. Chow et al, Structural, morphological, and magnetic study of nanocrystalline cobalt-copper powders synthesized by the polyol process, J. Mat. Res., **10** (6), p1546, 1995.

Harris et al[17] have synthesized copper-cobalt powders using a similar method. Their study is more comprehensive. They include XRD, EXAFS, and VSM analysis as means to characterize the resulting materials.

Another method for creating nano-crystalline copper-cobalt powders is mechanical alloying. Gente, Oehring, and Bormann[18] studied the mechanical alloying of copper and cobalt using XRD, SEM, and calorimetric measurements. They were able to create super-saturated solid solutions at concentrations much higher than those attained using equilibrium methods. Cabanas[19] et al have shown the lattice parameter of the copper-cobalt solid solutions varies as a function of milling time. Yoo and Yu[20] extend the same idea by applying magnetic measurements to the materials.

---

[17] V. G. Harris et al, Structure and magnetism of heat-treated nanocrystalline $Cu_{80}Co_{20}$ powders prepared via chemical means, J. Appl. Phys, **75** (10), p6610, 1994.
[18] C. Gente, M. Oehring, R. Bormann, Formation of thermodynamically unstable solid solutions in the Cu-Co system by mechanical alloying, Phys. Rev. B, **48** (18), p13244, 1993.
[19] J. G. Cabana-Moreno et al, Mechanical alloying of Co-Cu powder mixtures, Scr. Meta. et Mat., **28**, p645, 1993.
[20] Y. Yoo, S. Yu, W. Kim, Magnetic properties of nanocrystalline Cu-Fe-Co alloys processed by mechanical alloying, IEEE Trans. Mag., **31** (6), p3769, 1995.

Chapter 2. Experimental Techniques

Copper and cobalt powders were purchased commercially. The average particle size was reported by the manufacturer to be 4.9μm for the copper and 1.3μm for the cobalt powder. The purity of both powders was better than 99.6%. Both powders probably have a small oxide layer due to the nature of the packaging.

2.1. Powder into pellets

$Cu_{100-x}Co_x$ powders, for $0 < x < 5$, were carefully massed and stored in plastic vials. Next, 0.5wt% zinc stearate was added to each mixture for lubrication. The powders in the vials were then mixed in a "paint shaker" style SPEX 8000 mixer/mill for 10 minutes.

The powders were compacted in a SPEX 13mm diameter die to create cylindrical pellets. Because the load capacity of the die was 10 tons, we had to determine exactly how much load was required to generate dense pellets.

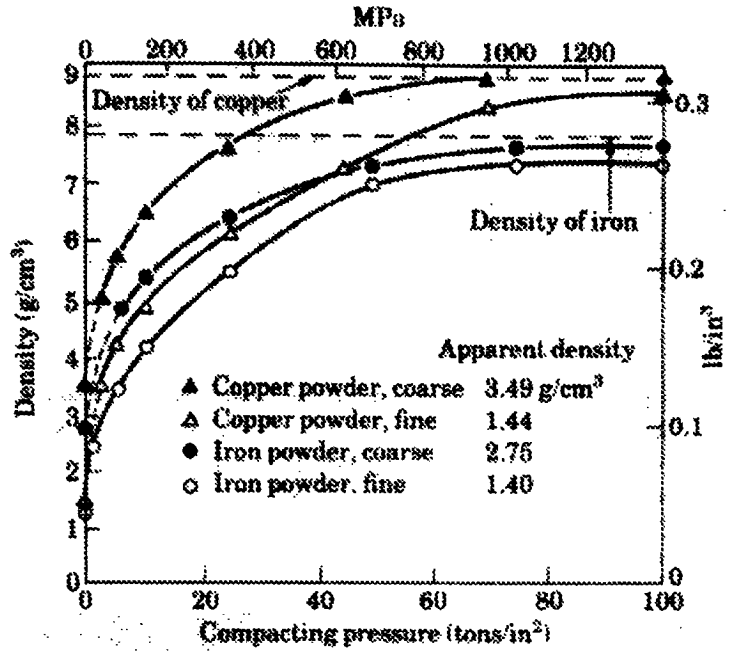

Figure 2.1. Density of copper and iron as a function of compacting pressure[1].

The pellets were pressed using a load of 5 tons, which results in a compacting pressure of about 25 tons/in^2. This load is safe for the die and should result in a pellet that is 83% dense (17% porous), as shown in Figure 2.1. Pellets were easily ejected from the die because of the lubrication provided by the small amount of zinc stearate.

The densities of some of these pellets are listed in Table 2.1. The stated porosity is calculated as $(1-\rho/\rho_{Cu})$, where $\rho_{Cu} = 8.92$ g/cm^3.

ID	mass (g)	d (mm)	h (mm)	ρ (g/cm³)	porosity (%)
A	5.21997	13.00	5.56	7.07	20.7
B	4.27499	13.00	4.54	7.09	20.5
C	4.90496	13.00	5.16	7.16	19.7
D	5.56580	13.00	5.88	7.13	20.0

Table 2.1. Pellet dimensions before solution treatment.

[1] S. Kalpakjian, Manufacturing Engineering and Technology, Addison-Wesley, p505.

2.2. Fabrication of Cu-Co solid solutions

2.2.1. Solution-annealing the pellets

In order to obtain a solid solution of cobalt in copper, we must find a temperature that is located above the solvus line for a given concentration. Figure 1.1 shows the binary phase diagram for copper-cobalt alloys.

To keep our alloying system dilute, we choose to work with 5wt% or less cobalt in copper. According to the phase diagram in Figure 1.1, the solvus temperature at 5wt% cobalt is 950°C. We choose to work at 1020°C to accelerate the diffusion process. However, the phase diagram does not indicate how long the heat-treatment must be in order to get this single phase.

To estimate the time required for the solution-treatment, we have developed a simple diffusion based model. Consider that we start with 5μm sized cobalt particles in a $Cu_{98}Co_2$ alloy. Imagine that each cobalt particle is evenly dispersed and enclosed within a cube of copper, as shown in Figure 2.2.

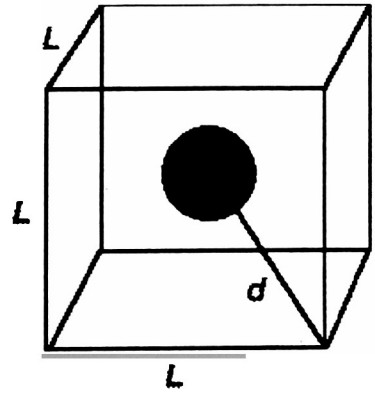

Figure 2.2. Cobalt particle imbedded in a solid copper matrix.

We determine L by defining it such that the cube contains 98wt% copper and 2wt% cobalt. The volume of the entire cube is written as

$$V = L^3 = V_{Co} + V_{Cu} \tag{2.1}$$

where V_{Co} is the cobalt particle volume and V_{Cu} is the volume of copper. Since we require the cube to have 98% copper, we can express the copper volume as follows

$$V_{Cu} = \frac{\rho_{Co} V_{Co}(0.98)}{\rho_{Cu}(0.02)}. \tag{2.2}$$

Using these relationships, we find the cube must be about 30μm on a side.

We can approximate the solution-treatment time by considering how long it will take for one cobalt atom to diffuse from the center of the cobalt particle to a corner of the cube. The distance d in this case is 25μm. Using an approximation of Fick's second law of diffusion[2] we find that

$$t = \frac{d^2}{4D_{Co \to Cu}}, \tag{2.3}$$

where $D_{Co\text{-}Cu}$ is the diffusion constant of a cobalt atom in copper and t is the time it takes to travel a distance d.

Referring back to Table 1.2, we find $D_{Co\text{-}Cu}$ is equal to 9.62×10^{-10} cm^2/s at a temperature of 1020°C. Using eq. (2.3) we find it takes about 5 minutes for a cobalt atom to travel from a cobalt particle to a corner of the cube. Therefore, we can treat

[2] W. F. Smith, Materials Science and Engineering, 2nd Ed., McGraw-Hill, p162, 1990.

this time as a "ball-park" estimate for the time required to put all cobalt in solid solution at 1020°C.

The pellets are loaded into a tungsten boat, four at a time. We choose a Lindberg tube furnace with a flowing argon atmosphere to reduce surface oxidation. The pellets are solution-treated at 1020°C for 60 minutes to obtain a sub-saturated solid solution (single phase). A time of 60 minutes is chosen to be sure a solid solution is obtained in the first try.

After the solution-treatment, the pellets are quenched in ice water to create a supersaturated solid solution. The time it took to remove the pellets from the furnace and immerse them in water averaged 3-5 seconds.

The size and mass of each pellet was recorded following the solution-treatment. It was found that both the height and diameter of the pellets decreased. Table 2.2 shows the dimensions of a few pellets which are representitive of all pellets.

mass' (g)	d' (mm)	h' (mm)	ρ' (g/cm^3)	porosity' (%)	% mass change	% d change	% h change
5.18980	12.10	5.24	8.56	4.1	0.58	6.62	5.76
4.25100	12.20	4.34	8.43	5.4	0.56	6.46	4.41
4.87582	12.20	4.92	8.53	4.3	0.59	6.46	4.65
5.53180	12.10	5.58	8.56	4.0	0.61	6.62	5.10

Table 2.2. Pellet dimensions following solution-treatment at 1020°C.

Table 2.2 indicates that after the solution-treatment, the density of each pellet approached the bulk density of copper. This was due to a shrinkage of both the diameter and height of the pellet.

In order to remove the oxide layer from each pellet, a mechanical polish using a 1μm α-Al_2O_3 slurry was performed. Although another oxide layer immediately forms, it is not thick enough to not affect subsequent measurements.

2.2.2. Calculation of the precise lattice parameter

In order to determine how much cobalt is in solution with copper, we examine the lattice parameter of Cu-Co solid solutions using x-ray diffraction. In the bulk, the lattice parameter of pure copper[3] is 3.61541A and the lattice parameter of fcc cobalt[4] is 3.544A. For a dilute Cu-Co solid solution, the lattice parameter is very close to that of bulk copper. Since we need to measure changes on the order of magnitude of parts per million (ppm) in the lattice parameter, we must develop a careful method for determining the lattice parameter of a Cu-Co solid solution.

To calculate the lattice parameter, we need to determine the locations of the diffraction peaks as precisely as possible. One way to insure this is to do a careful job collecting the data. The diffractometer was operated in "step mode". In this mode, the stepper moves to a given angle and pauses to collect data.

---

[3] B. D. Cullity, Introduction to Magnetic Materials, Addison-Wesley, 1972.
[4] J. R. Childress, C. L. Chien, Reentrant magnetic behavior in fcc Co-Cu alloys, Phys. Rev. B. 43 (10), p8089, 1991.

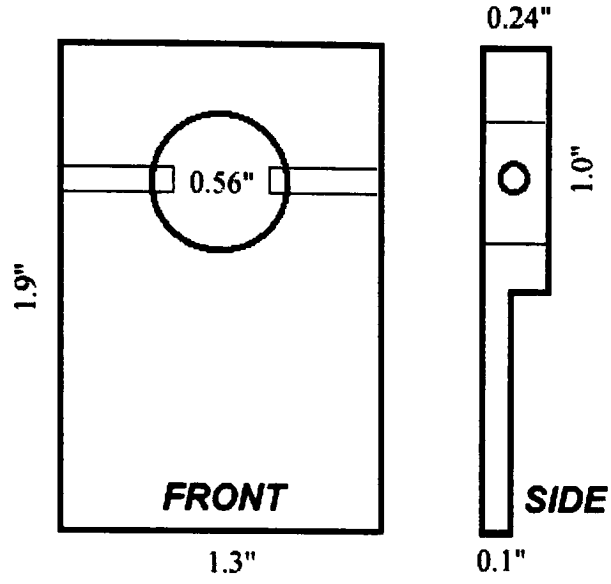

Figure 2.3. XRD sample holder schematic.

Another important experimental consideration is the sample position. The sample surface should be coincident with the diffractometer axis. To solve this problem, a special holder for the pellets was built, as shown in Figure 2.3. The holder permits the sample to be held flush with the holder surface. The holder was built such that the pellet would have a maximum exposure to the x-rays, resulting in the highest peak intensities. The pellet was held in place by two plastic pegs and leveled in the plane of the holder. This minimizes the sample displacement from the diffractometer axis.

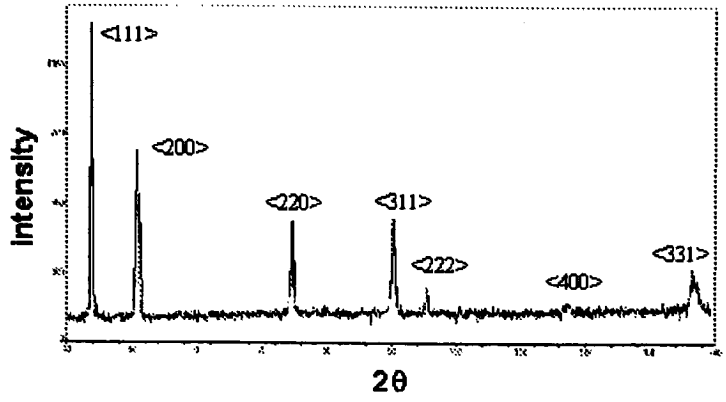

Figure 2.4. Sample diffraction pattern for a copper pellet, which is a plot of a relative diffracted x-ray intensity vs. collection angle.

After the XRD diffraction pattern for any given sample is acquired, we may then begin the analysis which leads to the precise lattice parameter. An example of a diffraction pattern for a Cu-Co solid solution is shown in Figure 2.4. The peaks are identified by the miller indices of their corresponding crystal planes.

Before curve fitting, intensity values were corrected for Lorentz Polarization and absorption effects.

$$I = \frac{I_{raw}}{LP} \tag{2.8}$$

where the correction factor is

$$LP = \frac{1+\cos^2 2\theta}{\sin^2\theta\cos\theta}. \tag{2.9}$$

Then, the corrected values were scaled by I_{max} to minimize round-off errors.

First, let us consider the x-ray source for the specific system used. The copper source emits x-rays of two different wavelengths[5], $\lambda_{K\alpha 1} = 1.540562A$ and $\lambda_{K\alpha 2} = 1.544390A$. The intensity of the $K\alpha_1$ peaks is approximately twice that of the $K\alpha_2$.

Taking this into consideration, we can consider each peak in the spectrum to be composed of two separate peaks. In order to accurately find the peak location, we may use a popular Pearson type VII curve fit[6].

The Pearson type VII function, Eq. (2.4), is a generalized function that describes the shape of XRD peaks very well.

$$PF(2\theta) = a\left(1+\frac{(2\theta - y)^2}{b}\right)^{-m} \tag{2.4}$$

where b is a constant related to the peak breadth, y is the location of the peak maxima, m is a shape factor, and a is the peak amplitude.

Since we must consider a more general case, our fitting function becomes the following,

$$I_{calc} = I_o + I_{K\alpha 1} + I_{K\alpha 2}$$

$$I_{calc} = I_o + a\left(1+\frac{(2\theta - y)^2}{b}\right)^{-m} + \frac{a}{2}\left(1+\frac{(2\theta - y - y_{sep})^2}{b}\right)^{-m} \tag{2.5}$$

where y_{sep} is the separation between the $K\alpha_1$ and $K\alpha_2$ peaks given by

[5] Jade v3.0 Data Aquisition software.
[6] S. K. Gupta, B. D. Cullity, Problems associated with K doublet in residual stress measurements, Advances in X-Ray Analysis, **23**, p333, 1980.

$$y_{sep} = \frac{6(\lambda_{K\alpha 2} - \lambda_{K\alpha 1})}{\lambda_{K\alpha 2} + 2\lambda_{K\alpha 1}} \tan\theta \,. \qquad (2.6)$$

The variable I_{OU} is the background intensity (assumed to be linear) with an arbitrary slope and intercept

$$I_o = s\theta + i \,. \qquad (2.7)$$

In Figure 2.6, we show an example of the spreadsheet used to fit this model to one peak.

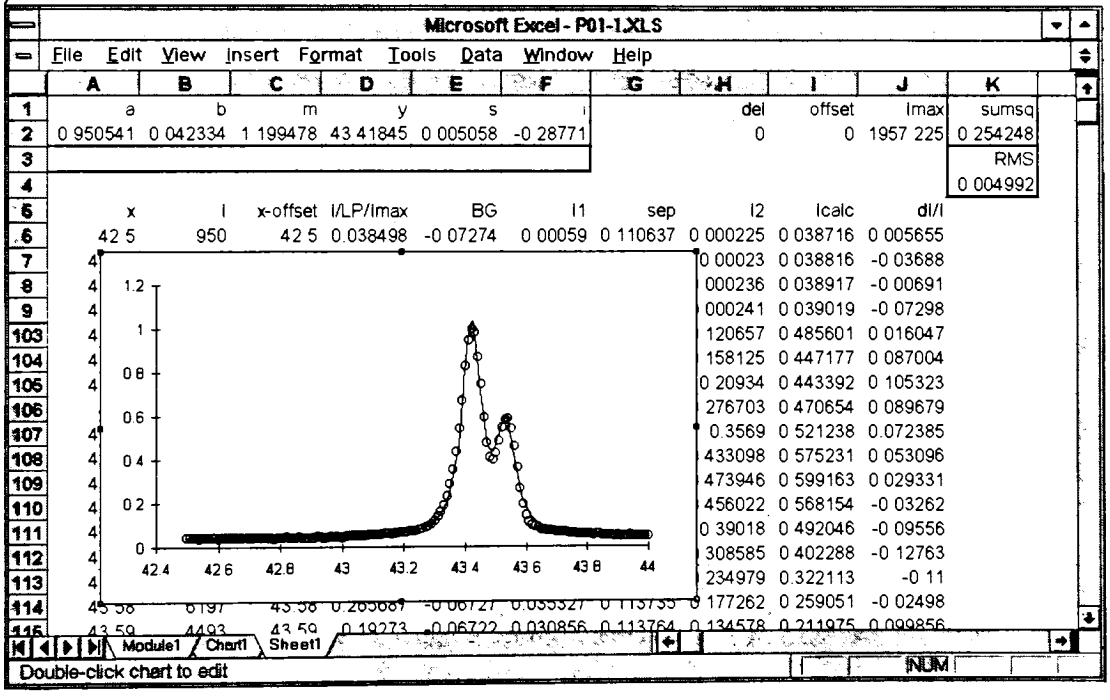

Figure 2.5. Sample spreadsheet used for determining the peak location in an XRD pattern.

Each peak in the XRD pattern was fit using the Solver function in Microsoft Excel, similar to what is shown in Figure 2.5. Sample results for one pattern are shown in

Table 2.3. In this table, we include the RMS value for each peak fit, which gives a rough estimate of the quality of the fit. The average RMS value is about 0.3%. This means that on the average, the best fit model only deviates from the raw data by about 0.3% per data point.

peak #	a	b	m	y	s	i	RMS
1	0.951	0.042	1.20	43.4185	0.0051	-0.288	0.003362
2	0.972	0.045	1.37	50.5360	-0.0001	-0.051	0.005234
3	0.929	0.061	1.99	74.2119	-0.0123	0.841	0.003724
4	0.923	0.066	1.87	90.0116	0.0072	-0.802	0.003857
5	0.660	0.064	1.60	95.2309	0.0072	-0.628	0.002631
6	0.474	0.111	2.30	116.9685	0.0065	-0.712	0.002438
7	0.766	0.096	1.17	136.5458	0.0140	-2.397	0.003069
8	0.768	0.121	1.10	144.7121	-0.0061	0.200	0.001722

Table 2.3. Example of the fitting results for one XRD pattern.

From the location of each peak, *y*, one can calculate a lattice parameter. However, the lattice parameter is more precise for higher angle peaks. A good way to determine the precise lattice parameter of a material is to calculate the lattice parameter *a*, from each peak (Table 2.4).

2θ (degrees)	d (A)	h	k	l	a (A)
43.4185	2.082424	1	1	1	3.606864
50.5360	1.804558	2	0	0	3.609115
74.2119	1.276799	2	2	0	3.611333
90.0116	1.089232	3	1	1	3.612574
95.2309	1.042841	2	2	2	3.612505
116.9685	0.903559	4	0	0	3.614237
136.5458	0.829189	3	3	1	3.614349
144.7121	0.808305	4	2	0	3.614850

Table 2.4. Summary of results for fitting of all 8 peaks in an XRD pattern.

One can then plot a for each peak versus $cos^2\theta/sin\theta$, as shown in Figure 2.6, and fit a straight line to the data. The y-intercept of this line is the precise lattice parameter a_o. The slope of this line indicates how far forward or back the sample surface was with respect to the diffractometer axis[7]. Thus, in Figure 2.6, a_o=3.61499A and R^2=0.98 the linear correlation coefficient indicating an excellent linear fit.

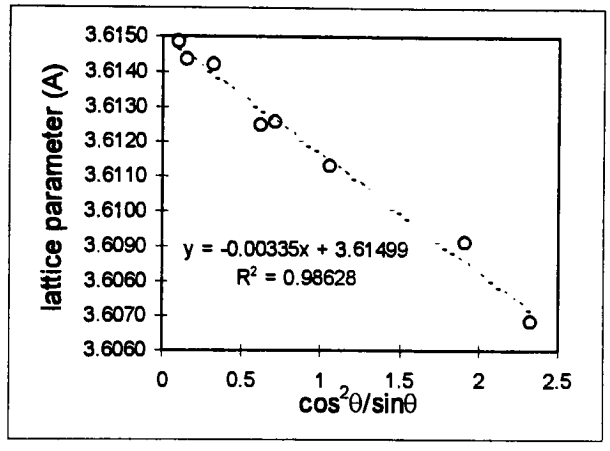

Figure 2.6. Determination of precise lattice parameter.

2.2.3. Checking for the presence of a complete solid solution

After the first solution-treatment, we must determine whether the material has reached its equilibrium state. We must also determine whether or not we have a single phase solid solution.

We solution-treat a few of the pellets for 60 more minutes at 1020°C. If the first heat-treatment was sufficient, we expect the lattice parameter to not change very much after the second anneal.

[7] B.D. Cullity, Elements of X-ray diffraction, Addison-Wesley, 1978.

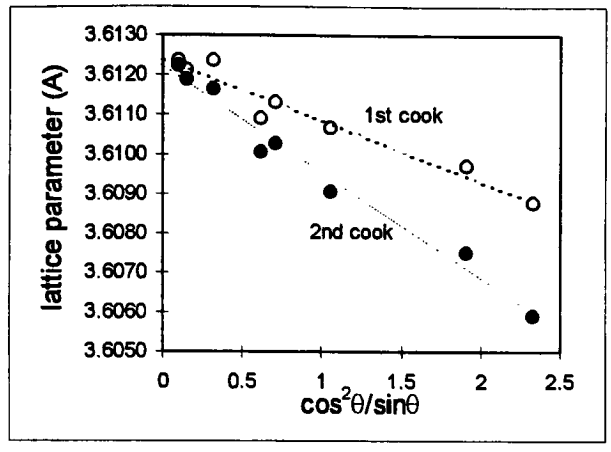

Figure 2.7. XRD results for same $Cu_{95}Co_5$ pellet solution-anneal for 60 and 120 minutes.

Figure 2.7 shows *a* vs. $\cos^2\theta/\sin\theta$ linear fits. Different slopes indicate different sample displacement. But nearly equal intercepts indicate no significant change in the precise lattice parameter.

The same procedure was also done for one more pellet. As the results listed in Table 2.5 show, the lattice parameters for both anneal times differ only by a few ppm.

pellet	a_o after 60 min (A)	a_o after 120 min (A)	% difference
$Cu_{95}Co_5$	3.61240	3.61223	0.005
$Cu_{98.5}Co_{1.5}$	3.61472	3.61474	0.0006

Table 2.5. Lattice parameter of two pellets after successive solution treatments.

Our results indicate that 60 minutes is sufficient for bringing the pellets to an equilibrium state at 1020°C.

Next, we wish to determine whether this equilibrium state, for each pellet, is indeed a complete solid solution. To do this, we exploit the fact that cobalt is intrinsically magnetic.

In the bulk and particulate form, cobalt behaves ferromagnetically (Figure 2.8b). Solid solutions of cobalt in copper (Figure 2.8a) behave paramagnetically. Paramagnetic materials have no coercivity and cannot be saturated using a common laboratory magnet. Therefore at a given applied field, the magnetization of a paramagnetic material is usually orders of magnitude smaller than the magnetization of a ferromagnetic material.

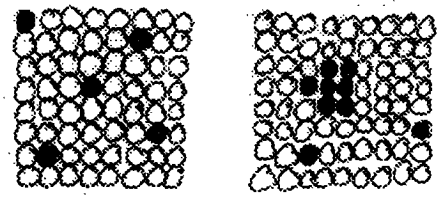

(a) (b)

Figure 2.8. (a) complete solid solution which is paramagnetic (b) a two phase material, solid solution and cobalt phase material which is ferromagnetic.

These ideas can be used to perform a simple test using a hand held permanent magnet. We put each solution-treated pellet near the permanent magnetic to see if there was an attraction. If there is an attraction, there are most likely a significant number of cobalt particles not dissolved into the copper lattice.

Another way to test for the presence of a complete solid solution is to measure the hysteresis loop for each pellet using VSM. The initial susceptibility of the pellets which exhibit paramagnetic properties is determined. Blannard and Turnbull[8] argue that the initial susceptibility of copper-cobalt solid solutions is proportional to the square of the cobalt concentration. This can be used as evidence for the existence of a complete solid solution and its paramagnetic behavior.

2.2.4. Determination of a lattice parameter calibration curve

Now that we have developed a method for preparing and testing for Cu-Co solid solutions, we must learn how the lattice parameter of the material depends on the cobalt concentration.

We fabricated and tested 20 pellets total, with 10 different cobalt concentrations. The pellet compositions are listed in Table 2.6.

$Cu_{100-x}Co_x$	number of pellets made
0.0	1
0.3	1
0.6	1
0.9	1
1.0	1
1.2	1
1.5	8
2.0	1
3.0	1
4.0	1
5.0	3

Table 2.6. Summary of the concentrations of pellets for this study.

[8] R. Tournier, A. Blandin, Influence of interactions between impurities on the appearance of magnetic moments in Cu-Co dilute alloys, Phys. Rev. Lett. **24** (8), p397, 1970.

2.3. Aging of pellets

The $Cu_{98.5}Co_{1.5}$ pellets were chosen for the aging process. From our VSM and XRD measurements, we were confident that these pellets were completely in a solid solution state after the solution-treatment. A dilute amount of cobalt in solution was also desirable because a magnetic argument, which is described later, assumes no particle interactions. Reducing the cobalt concentration increases the interparticle spacing between the cobalt precipitate particles.

A total of eight $Cu_{98.5}Co_{1.5}$ pellets were solution-treated. Four of the eight pellets were sectioned in half to yield a total of 12 samples. Each pellet was assigned a unique ID and heat-treated with a given time and temperature as shown in Table 2.7.

Pellet ID	time @ 700C (min)	Pellet ID	time @ 750C (min)
A	5	G1	5
D1	20	G2	20
C	41	E	41
B1	72	F	80
B2	136	H1	150
D2	250	H2	250

Table 2.7. Heat treatments for each pellet.

After the heat treatment, each pellet is quenched in ice water. The density of the pellets after the aging is found to be the same (within 1%) as before the aging.

2.4. Phase analysis after aging

2.4.1. Tracking cobalt precipitation using XRD

To analyze how much cobalt is **in** solid solution, we determine the lattice parameter of each pellet as previously mentioned in Section 2.2.2. From this lattice parameter, we can use the calibration curve determined in section 3.2 to predict how much cobalt is still in solid solution after the aging process.

2.4.2. Tracking cobalt precipitation using saturation magnetization

Next, we may use magnetometry methods for determining exactly how much cobalt has precipitated **out** of solution. The VSM is used to measure a hysteresis loop for each pellet.

The procedure for obtaining a hysteresis loop is to ramp the field from zero to a large positive field. The large field is then lowered and reversed to a large negative applied field. The field is then reversed one more time and driven to the high positive field again.

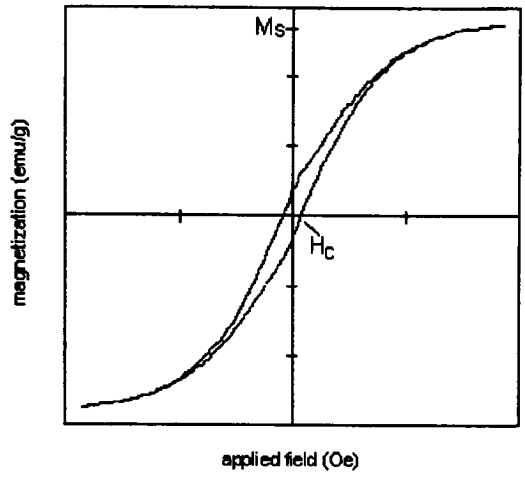

Figure 2.9. An example of a hysteresis loop for a ferromagnetic material.

From the hysteresis loop, many important magnetic quantities can be found. One of which is the saturation magnetization, M_s. This is the sample magnetization at high fields, which usually represents the value of the magnetization when all magnetic spins are aligned in the same direction. This quantity is a direct measure of how much cobalt has precipitated **out** of solid solution.

To emphasize this point, we show the magnetization curve for one pellet before and after the aging process in Figure 2.10. One can see that the magnetization of the pellet while in the solid solution state is two orders of magnitude smaller than after it is aged. Note that the scale of the primary axis on the left indicates the magnetization after aging and the secondary axis on the right indicates the sample magnetization before aging. The linear nature of the solid solution magnetization data indicates that it is paramagnetic, whereas after aging a ferromagnetic phase is present.

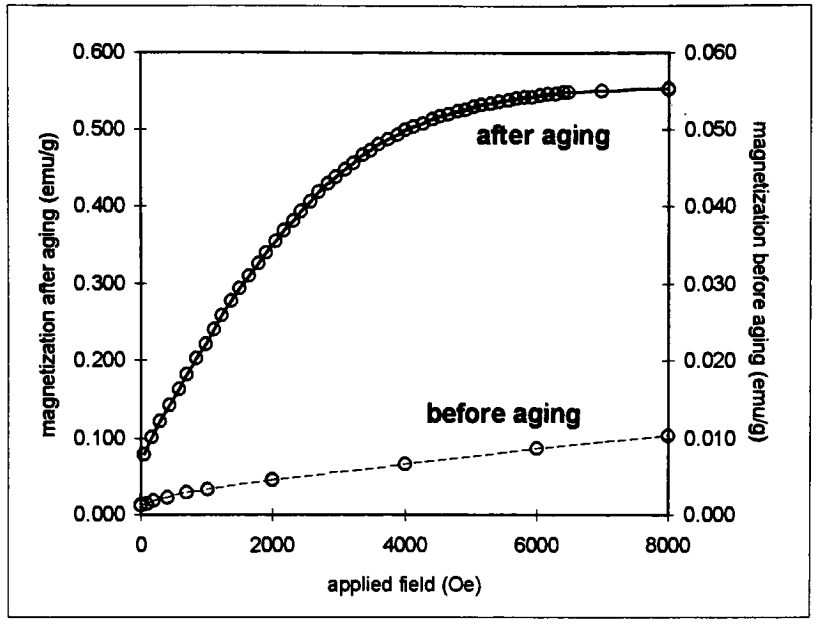

Figure 2.10. Magnetization curve for a pellet before and after and age of 41 minutes at 750°C.

2.5. Particle size analysis after aging

2.5.1. Determining particle size from coercivity

After we have characterized how much cobalt has precipitated out of solid solution, we would like to determine how large these cobalt precipitate particles are. Traditionally, there are many ways of doing this. However, since we are dealing with nanometer sized particles, we cannot use popular methods such as optical microscopy. Since the cobalt particles are magnetic, we may use magnetic methods to determine their size.

The coercivity of a material, H_c, is a measure of the reverse field required to reduce the magnetic moment of the sample back to zero after a large field is applied. For a random assembly of magnetic particles, the coercivity depends on the size, shape,

stress, spacing, and composition of the ferromagnetic particles. Therefore, if we hold everything constant except particle size, we can find a relationship between particle size and coercivity. This assumption is valid because the preparation of the pellets is the same except for the aging time and temperature. A hysteresis loop for a pellet aged for 41 minutes at 750C is shown in Figure 2.11. This hysteresis loop indicates indicates a coercivity of 275 Oe.

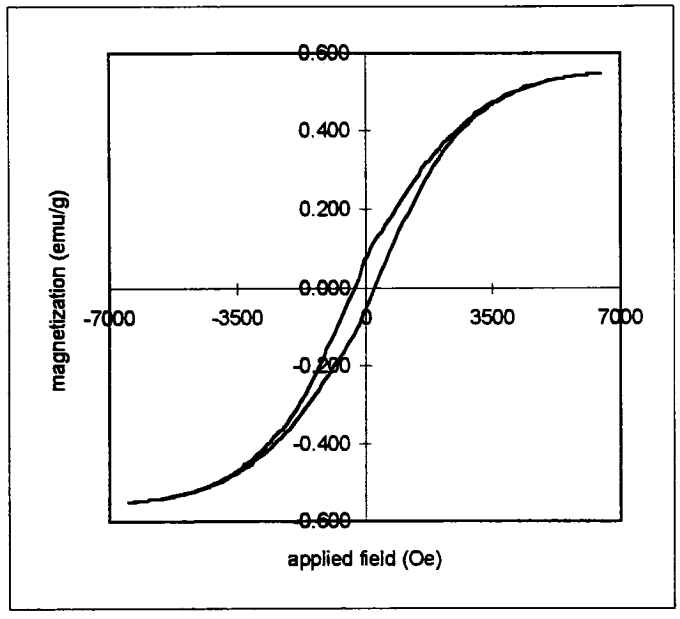

Figure 2.11. Hysteresis loop of a pellet aged for 41 minutes at 750C. This pellet has a coercivity of about 275 Oe.

Because there is some uncertainty associated with the field of the electromagnet around $H = 0$, we take the average of the coercivity on the left side and right side of the hysteresis loop. This uncertainty comes from a remanant magnetization in the electromagnet when there is no current turned on. There is also some error in the loop around $H = 0$ because the power supply is not bi-polar, so the leads must be switched twice during the run.

In order to understand the origin of the coercivity for the entire material, we first must understand the coercivity of a single particle. Below a certain critical diameter, d_p, the particle behaves super-paramagnetically. This means that the particle is small enough such that thermal energy keeps the particle from having a net magnetization.

If the particle is larger than d_p, the particle becomes single domain. A single domain particle is a particle with only one magnetic domain. In other words, the magnetic moments of each cobalt atom are all aligned in the same direction. The coercivity of one of these particles can be written as a function of the particle size[9] d,

$$H_c = H_{co}\left[1-\left(\frac{d_p}{d}\right)^{3/2}\right]; \qquad \text{for } d_p < d < d_s \tag{2.8}$$

where H_{co} is a constant.

As the particle becomes larger than another critical size, d_s, it becomes energetically favorable to break into multiple domains. When a particle is multi-domain, there is essentially no net magnetization in the absence of an applied field.

For our coercivity analysis, we will only consider particles in the single-domain and super-paramagnetic range. Figure 2.12 shows the general relationship between particle size d and coercivity H_{ci}.

[9] B.D. Cullity, Introduction to Magnetic Materials, Addison-Wesley, 1972.

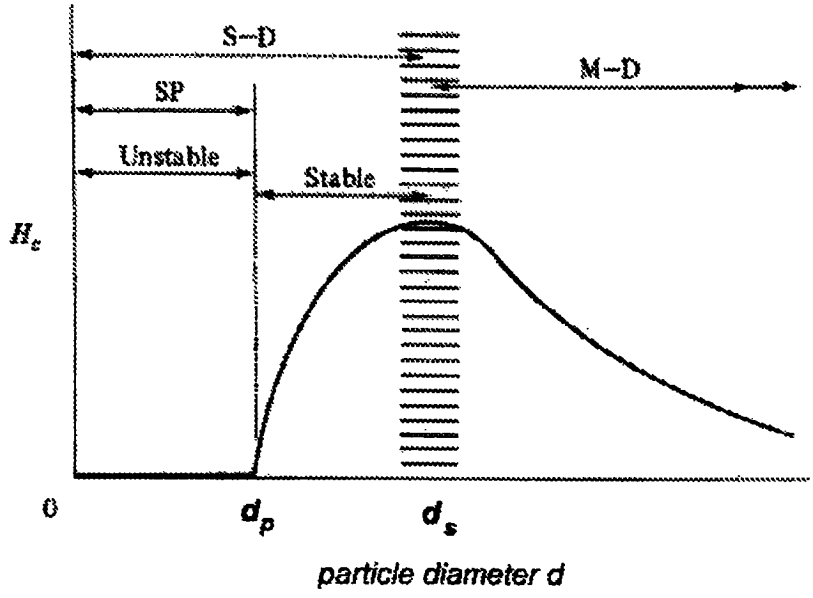

Figure 2.12. Relationship between coercivity and particle size for a ferromagnetic particle. S-D represents the single-domain region, M-D multi-domain region, and SP the superparamagnetic region[10].

2.5.2. Determining particle size using magnetic force microscopy

Magnetic force microscopy (MFM) is a new and powerful technique for imaging magnetic materials. We use MFM in this project to determine which pellets are in solid solution and to measure relative sizes of ferromagnetic cobalt precipitates.

The MFM rasters a magnetic tip over the sample surface. The tip experiences a measurable deflection as it passes over magnetic domains. The deflection of the tip is actually sensitive to the gradient of the stray magnetic fields produced by the sample. In other words, the resonant frequency of the cantilever is offset according to[11]

[10] B. D. Cullity, Introduction to Magnetic Materials, Addison-Wesley, 1966.
[11] T. R. Albrecht et al, Frequency modulation detection using high-Q cantilevers for enhanced force microscopy sensitivity, J. Appl. Phys. 69 (2), p668, 1991.

$$\Delta\omega = \frac{\omega_o}{2k}\left(\frac{\partial F_z}{\partial z}\right) \tag{2.9}$$

where F_z is the magnetic force exerted on the tip by the sample surface, k is the spring constant of the cantilever and ω_o is the resonant frequency of the cantilever.

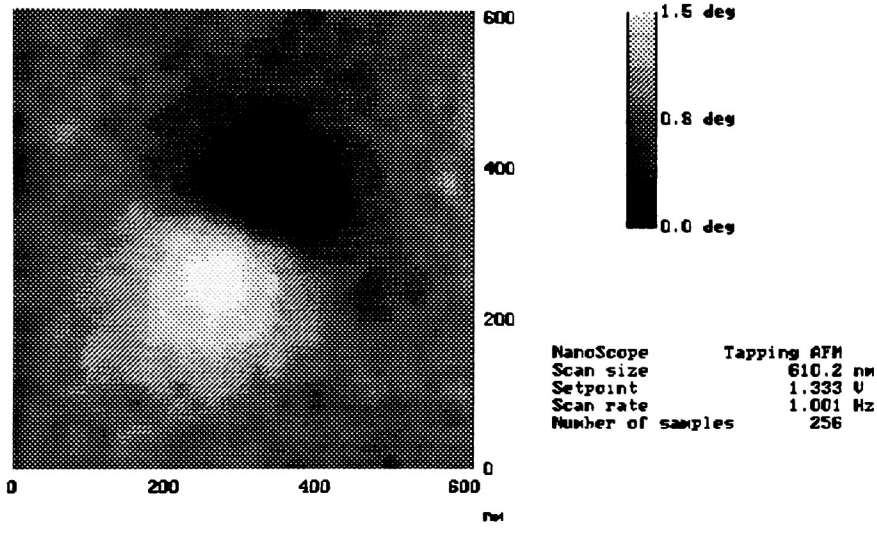

Figure 2.13a. MFM image of a single domain magnetic sphere. The scan size is approximately 600nm x 600nm. The particle magnetization vector is mostly in the plane of the page. The light and dark regions indicate the magnetization vector to be at about 75° with respect to the x direction.

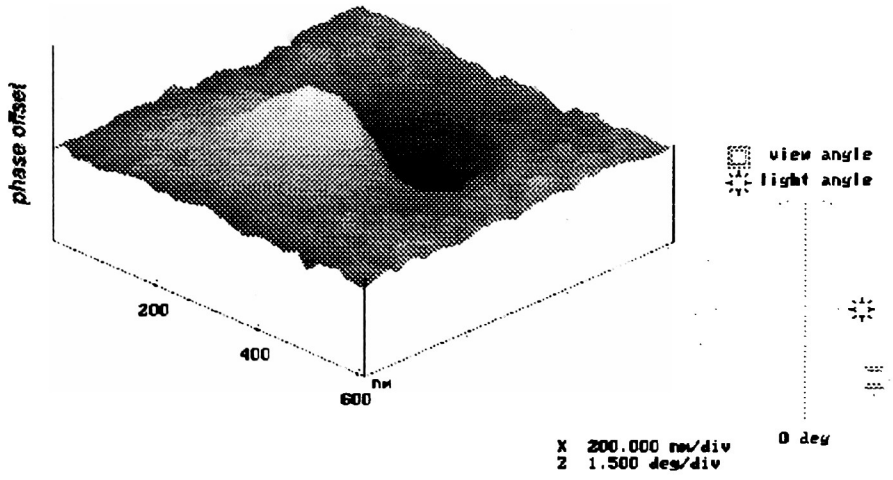

Figure 2.13b. MFM image of a single domain magnetic sphere plotted as a 3-dimensional surface. Scan size is approximately 600nm x 600nm.

In order to remove topographical information from the magnetic image, the MFM is operated in LiftMode. In this mode, the tip scans across the sample surface two times. The first scan operates in AFM mode to collect a topography profile. The second scan uses this topography profile to gather magnetic information at a constant height, known as the LiftHeight, above the sample surface.

Figures 2.13a and 2.13b show an MFM image characteristic of a single domain ferromagnetic particle. The image in Figure 2.13a shows a top-view plot of the MFM response. Light and dark areas represent the change in resonant frequency of the MFM tip. Notice that the light and dark regions indicate the direction of the particles magnetization vector, which is oriented approximately 75° with respect to the x direction. The image in Figure 2.13b shows a 3-dimensional surface plot of the same

data. In order to obtain meaningful information about the precipitate particle from the image, we must model the interaction between the tip and sample.

A simple method for approaching this problem is to start by making a few assumptions. We assume the particle to be imaged is single domain and spherical. In this case, we can treat the particle as a dipole located at the center of the sphere. Let us also assume that the MFM tip acts as a dipole.

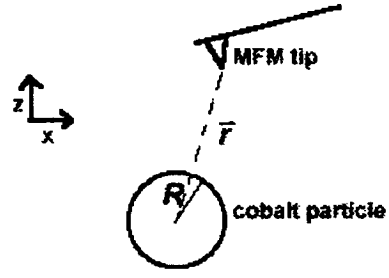

Figure 2.14. MFM tip-sample geometry, where *r* is the distance from the center of the particle to the MFM tip.

In Figure 2.14, the tip-sample geometry is shown. The distance from the center of the particle to the MFM tip is the distance *r*.

We must first calculate the magnetic field generated by the particle. For a dipole the field is written[12],

$$\vec{H}(r) = \frac{\vec{m}}{r^3} - \frac{3(\vec{m}\cdot\vec{r})\vec{r}}{r^5} \qquad (2.10)$$

[12] D. Saird, Scanning Force Microscopy, Oxford University Press, p158, 1991.

where r is the distance from the particle center (Figure 2.14), and m is the magnetization of the dipole (particle).

The particle magnetization can be expressed in terms of its x, y and z components

$$\vec{m} = m_x\hat{x} + m_y\hat{y} + m_z\hat{z}\,. \tag{2.11}$$

The force experienced by the tip is given by

$$\vec{F}(r) = -\nabla\left(\vec{m}_{tip}\cdot\vec{H}\right) \tag{2.12}$$

where m_{tip} is the magnetization of the tip.

Let us assume the tip magnetization is entirely in the z direction. Evaluating Eq. (2.12), we find the spatial gradient of the z component of the force experienced by the tip is written as,

$$\frac{\partial F_z}{dz} = k\left(\begin{array}{l}\dfrac{-105z^3\left(m_x x + m_y y + m_z z\right)}{\left(x^2+y^2+z^2\right)^{9/2}} + \dfrac{45m_z z^2}{\left(x^2+y^2+z^2\right)^{7/2}} + \\ \dfrac{45z\left(m_x x + m_y y + m_z z\right)}{\left(x^2+y^2+z^2\right)^{7/2}} - \dfrac{9m_z}{\left(x^2+y^2+z^2\right)^{5/2}}\end{array}\right). \tag{2.13}$$

In this case, the constant k is dependent on m_{tip} and the particle volume. If one assumes the tip magnetization is constant, the constant k can be used as a relative measure of particle size, from particle to particle.

We can now fit our experimental data to equation (2.13) using the solver function in Microsoft Excel. In the calculation, we fit the following parameters:

- z tip-particle center distance
- x_o, y_o x and y image offsets
- m_x, m_y, m_z precipitate particle magnetization vectors
- k constant coefficient, depending on m_{tip} and particle volume
- o gray-level offset of MFM image.

In order to test the validity of our model, we imaged the same cobalt particle at 6 different lift heights. If our model is valid, we should expect a 1:1 correspondence between the MFM lift height and the z parameter obtained from our model.

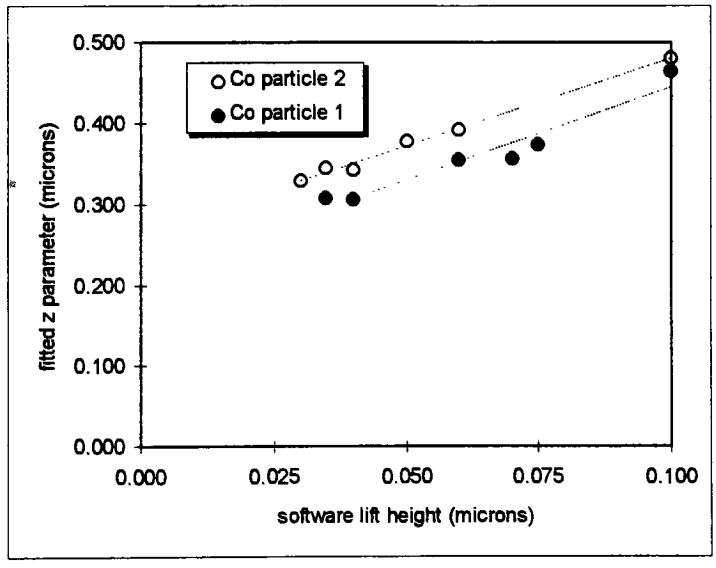

Figure 2.15. Relationship between MFM lift height and fitted z for 2 different single-domain cobalt particles.

Instead, we find a 1:2 correspondence between the MFM lift height and the fitted z parameter from our model for two separate particles (Figure 2.15). We also find a 1:3 correspondence for one additional particle imaged. There is also some dependence of

the fitted particle size as a function of lift height. In theory, we should expect the same particle size from any height.

Recall that our model assumes the tip magnetization is all in the z direction. We altered our model to consider an additional tip magnetization component, perpendicular to the z direction. Our model then becomes more complicated

$$\frac{\partial F_z}{dz} = k_z \left(\frac{-105z^3\left(m_x x + m_y y + m_z z\right)}{\left(x^2+y^2+z^2\right)^{9/2}} + \frac{45m_z z^2}{\left(x^2+y^2+z^2\right)^{7/2}} + \frac{45z\left(m_x x + m_y y + m_z z\right)}{\left(x^2+y^2+z^2\right)^{7/2}} - \frac{9m_z}{\left(x^2+y^2+z^2\right)^{5/2}} \right) + k_p \left(\frac{-105yz^2\left(m_x x + m_y y + m_z z\right)}{\left(x^2+y^2+z^2\right)^{9/2}} + \frac{30m_z yz}{\left(x^2+y^2+z^2\right)^{7/2}} + \frac{15m_y z^2}{\left(x^2+y^2+z^2\right)^{7/2}} + \frac{15y\left(m_x x + m_y y + m_z z\right)}{\left(x^2+y^2+z^2\right)^{7/2}} - \frac{3m_y}{\left(x^2+y^2+z^2\right)^{5/2}} \right) \tag{2.14}$$

where k_z is a constant that depends on z component and k_p a constant that depends on the x-y planar component of the tip magnetization. Table 2.8a shows the fitting results for a given particle at different lift heights using our regular model. Table 2.8b shows the fitting results for the same particle and lift heights using our modified model. The values in the error column are the root-mean-square of the difference between the model and the experimental data.

lift height (nm)	k	z (nm)	error
0.030	0.0083	0.329	3.36
0.035	0.0043	0.346	3.22
0.040	0.0025	0.344	3.05
0.050	0.0041	0.379	2.36
0.060	0.0019	0.392	2.43
0.100	0.0044	0.480	2.17

Table 2.8a. Results for fitting our model to the same particle at various lift heights.

lift height (nm)	k_z	k_p	z (nm)	error
0.030	0.00198	-0.00010	0.334	3.28
0.035	0.00324	-0.00025	0.333	3.06
0.040	0.00251	0.00001	0.344	3.05
0.050	0.00440	-0.00017	0.381	2.34
0.060	0.00187	-0.00014	0.395	2.28
0.100	0.00300	-0.00003	0.470	2.06

Table 2.8b. Results of fitting our modified model to the same particle at various lift heights.

Note that the planar component k_p of the tip magnetization is very small compared to the z component k_z. This leads us to believe that considering a component other than in the z direction for the tip magnetization complicates the model with no benefits.

Chapter 3. Results and Discussion of Cu-Co Solid Solutions

Cu-Co pellets, of various concentrations, are solution-annealed for 60 minutes at 1020C. We use vibrating sample magnetometry to determine what magnetic state each pellet is in. The magnetic state indicates whether or a not a single phase solid solution exists. We also use x-ray diffraction to measure the lattice parameter of each pellet. For Cu-Co solid solutions, the lattice parameter indicates how much cobalt is in solution.

3.1. Magnetic properties of Cu-Co solid solutions

We found the magnetic properties of the solution-treated Cu-Co pellets to depend on the cobalt concentration. The pellets with 2% or less cobalt behaved paramagnetically. For paramagnetic solid solutions, we expect the initial susceptibility to be proportional to the cobalt concentration squared[1]. Our results, shown in Figure 3.1, are consistent with this idea.

[1] R. Tournier, A. Blandin, Influence of interactions between impurities on the appearance of magnetic moments in copper-cobalt dilute alloys, Phys. Rev. Lett., **24** (8), p397, 1970

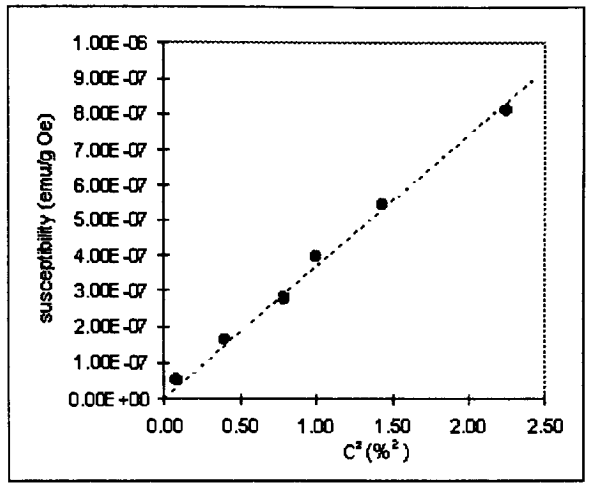

Figure 3.1. Initial susceptibility of Cu-Co solid solutions as a function of cobalt concentration.

The initial susceptibility X_o of each pellet was determined by fitting a straight line to the magnetization data measured using a VSM.

$$X_o = \frac{\sigma}{H} \tag{3.1}$$

where σ is the sample magnetization (in emu/g) and H is the applied magnetic field.

The magnetization did not completely extinguish at zero field. We believe this is due to a small ferromagnetic component residing in the material. However, a simple calculation shows the ferromagnetic component constitutes less than 0.01% of the entire material.

The pellets with 3% or more cobalt behaved ferromagnetically. This means their magnetic moment was easily saturated in the lab. Recall, that from this magnetic

moment, one can calculate the concentration of the ferromagnetic phase using the saturation magnetization.

$$c = \frac{\sigma_{pellet}}{\sigma_{Co}} \tag{3.2}$$

where σ_{pellet} is the saturation magnetization of the pellet and σ_{Co} is the bulk magnetization value of fcc cobalt (172emu/g[2]).

Our results for each pellet are shown in Figure 3.2. Notice that for the 0-2% cobalt pellets, VSM measurements show that all cobalt is in solid solution. However, for each pellet with 3-5% cobalt, there is only about 2% in solution.

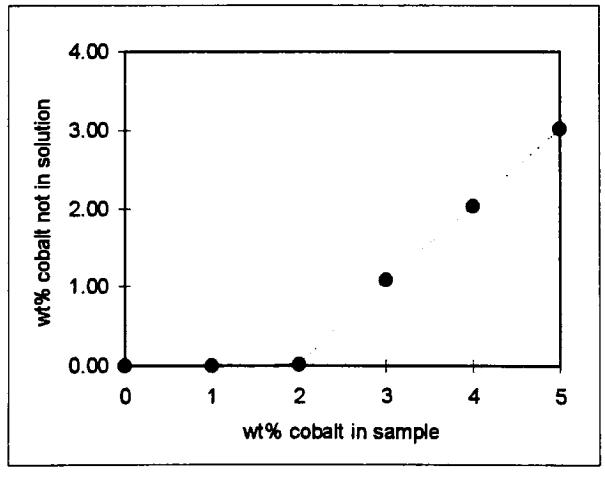

Figure 3.2. Amount of ferromagnetic cobalt in solution-annealed Cu-Co pellets determined from VSM measurements.

[2] J. R. Childress, C. L. Chien, Reentrant magnetic behavior in fcc Cu-Co alloys, Phys. Rev. B, 43 (10), p8089, 1991

The VSM measurements are validated by performing a simple magnet test. Each pellet is held up to a strong permanent magnet. If the pellet is attracted, it must have an appreciable ferromagnetic phase. On the other hand, if the pellet does not feel an attractive force, there is evidence that the pellet is paramagnetic (complete solid solution). This is because the magnetic moment of a paramagnet is a few orders of magnitude smaller than that of a ferromagnet.

Therefore, from the magnetic properties of each solution-annealed Cu-Co pellet, we find that 2% cobalt is the most that can be retained in solid solution with copper. The Cu-Co binary phase diagram and calculations by Servi and Turnbull suggest that 4% or more cobalt can be put into solid solution at the annealing temperature. This discrepancy may be due to our heat-treating methods. Impurities may also be affecting the solubility of cobalt in copper.

3.2. Crystalline properties of Cu-Co solid solutions

Each solution-annealed Cu-Co pellet was analyzed using an X-ray diffractometer. We calculated the lattice parameter of the pellets using the methods described in Section 2.2.2.

Our results are shown in Figure 3.3. We found that in general, the Cu-Co solid solution lattice parameter decreased as the cobalt concentration increased. This is

expected, because the atomic radius of cobalt (0.125nm) is slightly smaller than that of copper (0.128nm).

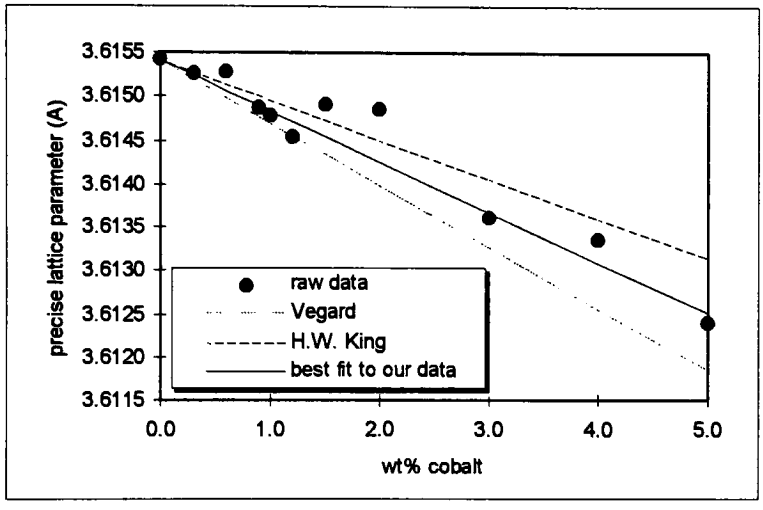

Figure 3.3. Lattice parameter of solution-annealed Cu-Co pellets as a function of cobalt concentration. Included, are the results predicted by H.W. King and Vegard's law.

We have included the results predicted by Vegard's Law[3] and H.W. King[4] for comparison to our data. Vegard's law states that there is a linear relationship between the lattice parameter and solute concentration. This law assumes unlimited solid solubility for the alloy.

H. W. King has reported on a modified model. He considers a finite solid solubility of cobalt in copper and gives quantities he identifies as quantitative size factors. These

[3] W. F. Smith, Materials Science and Engineering, 2nd Ed., p162, 1990.
[4] H. W. King, Quantitative size-factors for metallic solid solutions, J. Mat. Sci., 1, p79, 1966.

size factors can be used to calculate the lattice parameter of the Cu-Co system as a function of cobalt concentration.

In other words, we can calculate the lattice parameter of the Cu-Co alloy as a function of the cobalt concentration c,

$$a_{Cu-Co}(c) = a_{Cu}(1 + lsf \cdot c) \tag{3.2}$$

where a_{Cu} is the lattice parameter of copper and lsf is a linear size factor. This linear size factor provides a simple numerical way to understand how the cobalt content affects the Cu-Co solid solution lattice parameter.

Using this argument, we can quantitatively compare our results to those predicted by Vegard's law and H.·W. King.

source	lsf (%)
Vegard's law	-1.98
H.W. King	-1.26
our data: 0-2wt%	-1.00
our data: 0-5wt%	-1.61

Table 3.1. Linear size factors of Cu-Co solid solutions.

One can see by the results listed in Table 3.1 that our data does not agree with literature values. We have calculated a linear size factor for our data over two ranges of cobalt concentration, 0-2% and 0-5%. In that complete solid solutions probably do not exist in excess of 2% cobalt, we would like to know the linear size factor in the range 0-2%.

Because we are looking for lattice parameter variations on the order of ppm, we need to understand the repeatability of our results. To determine the repeatability of a given measurement for the same pellet, we completed the measurement and analysis procedure a total of 4 times for the same pellet.

scan number	lattice parameter (A)
1	3.61509
2	3.61504
3	3.61499
4	3.61507

Table 3.2. Lattice parameter of pellet E, aged 41min at 750°C, for four different measurement runs.

This data, listed in Table 3.2, indicates a measurement repeatability of +/- 0.00005A. This is very good because a repeatability better than +/- 0.00005A was not expected with the diffractometer. Next, we wished to determine the repeatability of the lattice parameter of different pellets, prepared under the same experimental conditions. For this test, we used the results for 8 different $Cu_{98.5}Co_{1.5}$ pellets.

pellet ID	lattice parameter (A)
A	3.61499
B	3.61474
C	3.61466
D	3.61522
E	3.61482
F	3.61496
G	3.61480
H	3.61517

Table 3.3. Lattice parameter of solution-annealed $Cu_{98.5}Co_{1.5}$ pellets.

From this data in Table 3.3, we determine a pellet-pellet repeatability of +/- 0.00017A. This shows there is a significant uncertainty associated with any given lattice parameter calculation.

3.3. Discussion of Cu-Co solid solutions

Magnetic measurements indicate that all Cu-Co pellets with 2% or less cobalt were complete solid solutions. The same measurement on pellets with 3% or more cobalt suggested the presence of a ferromagnetic phase of cobalt particles. On the other hand, x-ray diffraction analysis hints that we may be getting as much as 5% cobalt into solid solution during our solution-treatment, in that the lattice parameter decreases in a linear fashion for all cobalt concentrations studied.

The magnetic measurements are concrete and conclusive. There is no second guessing that the saturation magnetization is a measure of how much cobalt is not in solid solution. However, the x-ray analysis is less conclusive.

Taking into consideration the VSM analysis, one would expect the curve in Figure 3.3 to level for cobalt concentrations greater than 2%. This is not the case. One reason why the lattice parameter continues to decrease in a linear fashion is there may be a significant amount of impurities in the pellets. EDXA showed the presence of

Titanium particles averaging 1μm in size. These impurities may be also entering into a solid solution with copper, effectively blocking all of the cobalt from doing the same.

Although the solvus curve described by Servi and Turbull predicts we can dissolve 4.3% cobalt in copper at the solution-anneal temperature, this does not mean it is possible for this alloy. This system has a lower solubility limit because of the less than ideal experimental and materials conditions. The initial powders obtained were low grade, and probably had a significant oxide coating.

Chapter 4. Results and Discussion of Precipitates in Cu-Co Alloys

For the aging process, $Cu_{98.5}Co_{1.5}$ alloys were chosen. Previous XRD and VSM analysis predicts that our solution-annealing process is sufficient to generate a solid solution for this concentration. These pellets were aged at 700C and 750C for times ranging from 5-250 minutes. To study the phases that result from the aging heat-treatments, we use XRD, VSM and MFM. X-ray diffraction results depend on the amount of cobalt **in** solid solution. The VSM results depend on the amount of cobalt **out** of solution and the size of the precipitates. Magnetic force microscopy images depend on the size and shape distribution of the precipitates.

4.1. Magnetic properties of cobalt precipitates in aged Cu-Co

4.1.1. Phase and size analysis using vibrating sample magnetometry

Using the vibrating sample magnetometer (VSM), a hysteresis loop was acquired for each pellet. To test the uniformity of the magnetic properties throughout the pellet, a small piece was sectioned off and measured. The magnetic properties of the section were identical to that of the whole pellet, indicating a uniform precipitate dispersion.

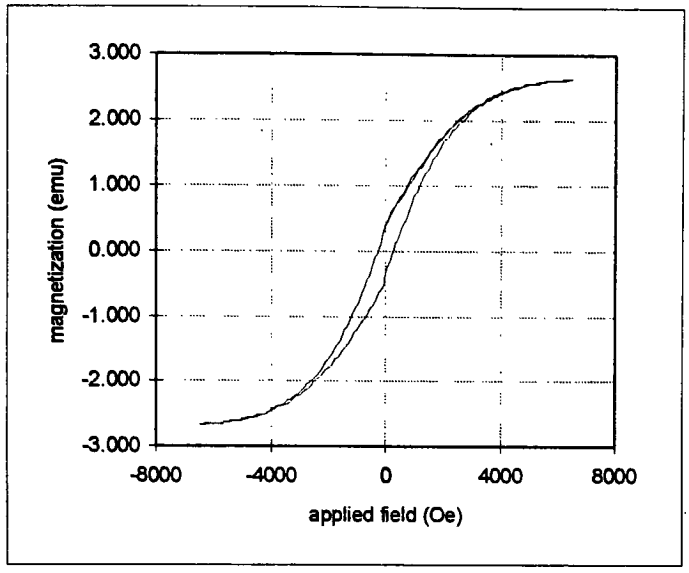

Figure 4.1. Hysteresis loop for a $Cu_{98.5}Co_{1.5}$ pellet aged 250min at 700°C.

An example of a hysteresis loop for a $Cu_{98.5}Co_{1.5}$ pellet aged 250min at 700°C is shown in Figure 4.1. In this plot, note that where the curve crosses the x-axis is where the coercivity of 275 Oe is calculated from. This coercivity measurement is repeatable to about +/- 10 Oe. In addition, the location on the magnetization axis where the curve crosses is known as the remanance. In this case, the remanance is about 10% of the saturation magnetization.

From the hysteresis loop, one may use the saturation magnetization of each pellet to determine the amount of cobalt precipitated out of solid solution.

$$\%\ cobalt\ out\ of\ solution = \frac{\sigma_s}{\sigma_{Co}}.$$

For this calculation, we assume the bulk magnetization of fcc cobalt, σ_{Co}, is 172emu/g. In Figure 4.2, we show the amount of cobalt precipitated out of solution

as a function of aging time and temperature. A curve of the following general form is fit to the data for calculational purposes,

$$\% \text{ cobalt out of solution} = at^{\gamma} \tag{4.1}$$

where a and γ are constants and t is time.

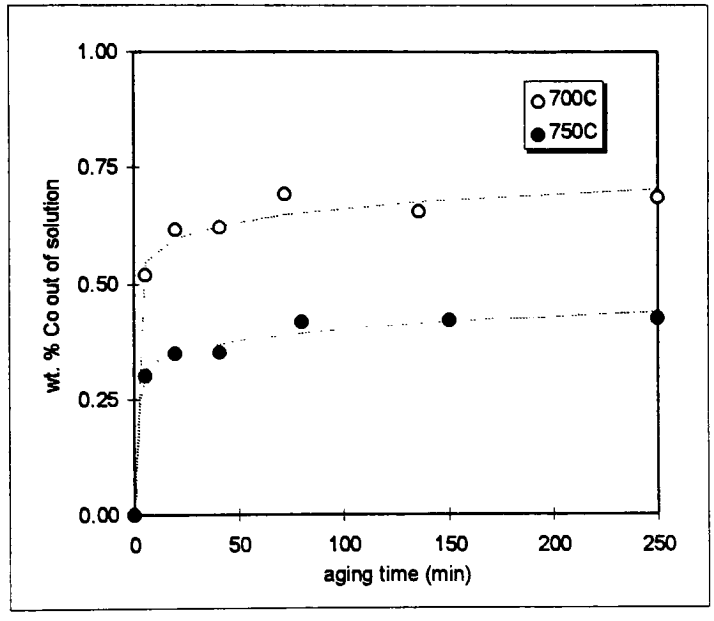

Figure 4.2. Amount of cobalt precipitated out of solution for various aging time and temperatures.

For aging times greater than 20 minutes, the precipitation process is nearly complete. For both aging temperatures, the amounts of cobalt out of solid solution approach the values predicted by the solvus line of Servi and Turbull as shown in Table 4.1. For comparison, we also show our solid solubility at the solution anneal temperature compared to what is expected.

aging temperature (C)	our solid solubility (%)	Servi and Turbull solid solubility (%)	percent difference
700	0.798	0.791	0.9%
750	1.064	1.103	3.5%
1020	1.96	4.261	54%

Table 4.1. Solid solubility of cobalt in copper at various temperatures.

The coercivity of each pellet is shown in Figure 4.3. This quantity can tell us something about the size of the cobalt precipitates.

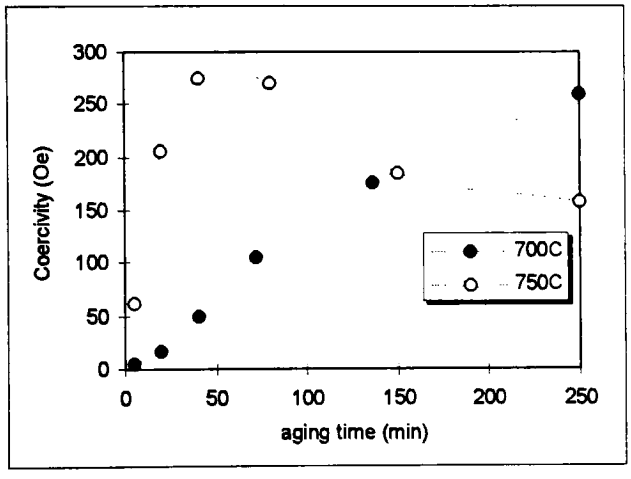

Figure 4.3. Coercivity of each pellet aged at 700C and 750C as a function of aging time.

A relationship between particle size and coercivity was described in detail in Section 2.5.1. However, we also need to relate the particle size to aging time and temperature if we are to effectively understand this process.

Several investigators have developed specific models for the growth of cobalt particles. We, however, will adopt a more generalized approach. We will consider a simple growth rate given by

$$d = d_o + \alpha\, t^{\gamma}, \tag{4.2}$$

where t is time and α, d_o, and γ are constants.

The constant α is the only temperature dependent term in the model. If this term is a measure of the growth rate at different temperatures, it must depend on how fast the cobalt atoms can travel and the concentration of cobalt atoms in solid solution. We consider the amount of cobalt in solid solution, because if there are more particles mediating the growth process, it should occur at a faster rate. We can express these ideas mathematically,

$$\alpha = k\left(c_s D_{Co \to Cu}\right), \tag{4.3}$$

where $D_{Co\text{-}Cu}$ is the diffusivity and c_s the solubility of cobalt in copper at a given temperature, and k is a constant.

We may now express the coercivity as a function of the particle size found using Eq. (4.2),

$$H_c = H_{co}\left[1 - \left(\frac{d_p}{d}\right)^{3/2}\right], \qquad \text{for } d_p > d > d_s \tag{4.4}$$

where H_{co} is a constant and d_p is the critical size for superparamagnetic behavior (70A).

We use the Solver function in Microsoft Excel to find the correlation between our time and coercivity data. In Figure 4.4, the spreadsheet used for this fit is shown. In the

the top left hand corner are the fitting variables, d_o, α_{700}, α_{750}, γ, and H_{co}. In the main table in the spreadsheet, notice separate columns where Eqs. (4.2) and (4.4) are used to calculate a fitted d and H_c. The condition of the "best fit" model is one in which the difference between the fitted H_c and the measured H_c is minimized. Notice that only the raw data believed to be representative of cobalt particles in the size range $d_p > d > d_s$ are used.

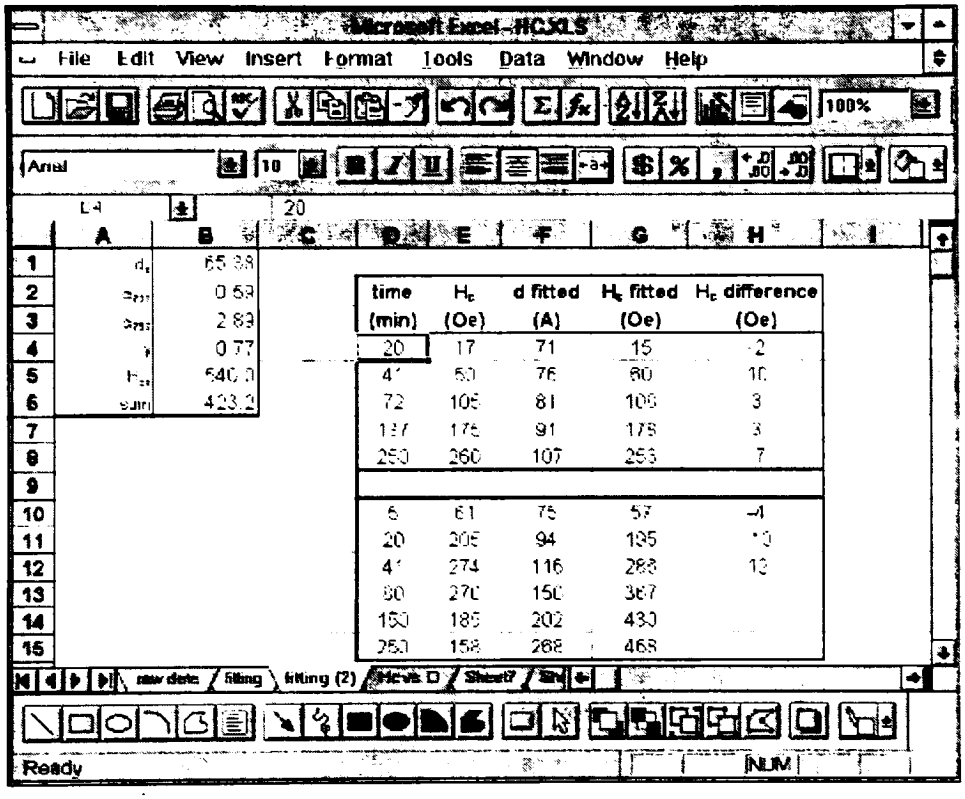

Figure 4.4. Excel spreadsheet used to find a correlation between coercivity and aging time and temperature. A result of the fit is an effective particle size as a function of aging time and temperature.

A result of the fit will be an effective particle size as a function of time. A summary of the fitting result is shown in Table 4.2.

variable	value
d_o	65.4 A
α_{700}	0.59
α_{750}	2.89
γ	0.77
H_{co}	540 Oe

Table 4.2. Fitting parameters for determining precipitate particle size from coercivity.

Our model predicts the ratio $\alpha_{750}/\alpha_{700}$ to be 4.9. Using the literature values for c_s and $D_{Co\text{-}Cu}$ at both temperatures in Eq (4.2), in we expect this ratio to be 5.1. This provides some evidence that our model may be correct.

Using these results, we may graphically depict the precipitate particle growth. In Figure 4.5, we show the "effective" particle size determined from our coercivity and growth model as a function of aging time and temperature.

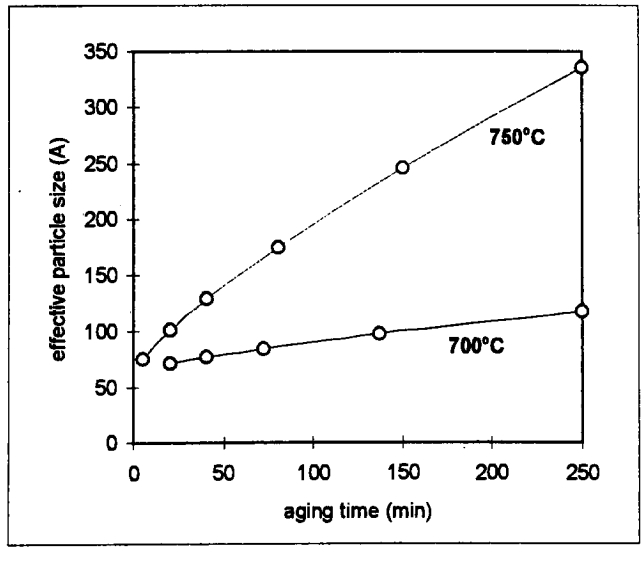

Figure 4.5. Cobalt precipitate size determined from coercivity measurements.

We also note that the remnant magnetization (magnetization in the absence of an applied magnetic field) is on the order of 10-20% of the saturation magnetization. For a narrow distribution of single domain particles, theory predicts the a value of about 48%. The reason for our remnant magnetizations being low is probably due to a very wide particle size distribution. It is likely that for most aging temperatures, there are still many cobalt particles that are in the superparamagnetic size range. These superparamagnetic particles have no remnant magnetization, which may explain the values between 10-20% we have measured.

4.1.2. Size analysis using magnetic force microscopy

The polished side of each pellet was then analyzed using magnetic force microscopy (MFM). MFM analysis on each pellet yielded images with either no magnetic contrast, all single-domain particles, or some single-domain and multiple-domain particles. Table 4.3 lists what type of image was found for each pellet.

aging temperature (C)	aging time (min)	MFM results
700	5	NP
700	20	NP
700	41	NP
700	72	SD
700	136	SD
700	250	SD
750	5	NP
750	20	SD
750	41	SD
750	80	SD
750	150	MD
750	250	MD

Table 4.3. MFM results for each pellet. *NP*: no particles, *SD*: single-domain, *MD*: single-domain and multi-domain.

For each pellet that yielded ***SD*** results (3 for each aging temperature), we performed the following analysis. From the MFM image, anywhere between 5 and 8 particles were isolated for analysis. Each individual particle was then fit to the MFM model described in detail in Section 2.5.2. The constant, k, fitted for each particle is proportional to the particle volume. We then find a relative average particle size for each pellet using the formula,

$$D_{avg} = \frac{\sum_{i=1}^{n} k_i^{1/3}}{n} \tag{4.4}$$

where n is the number of particles analyzed for a given pellet.

An example of a SD image is shown in Figure 4.6.

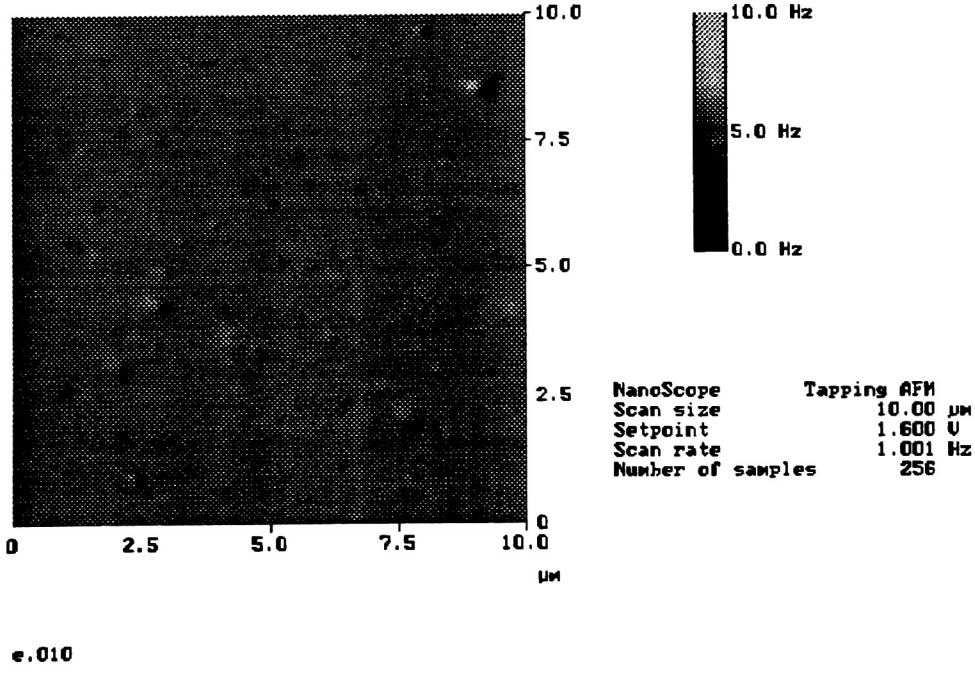

Figure 4.6. A SD MFM image of cobalt particles in copper.

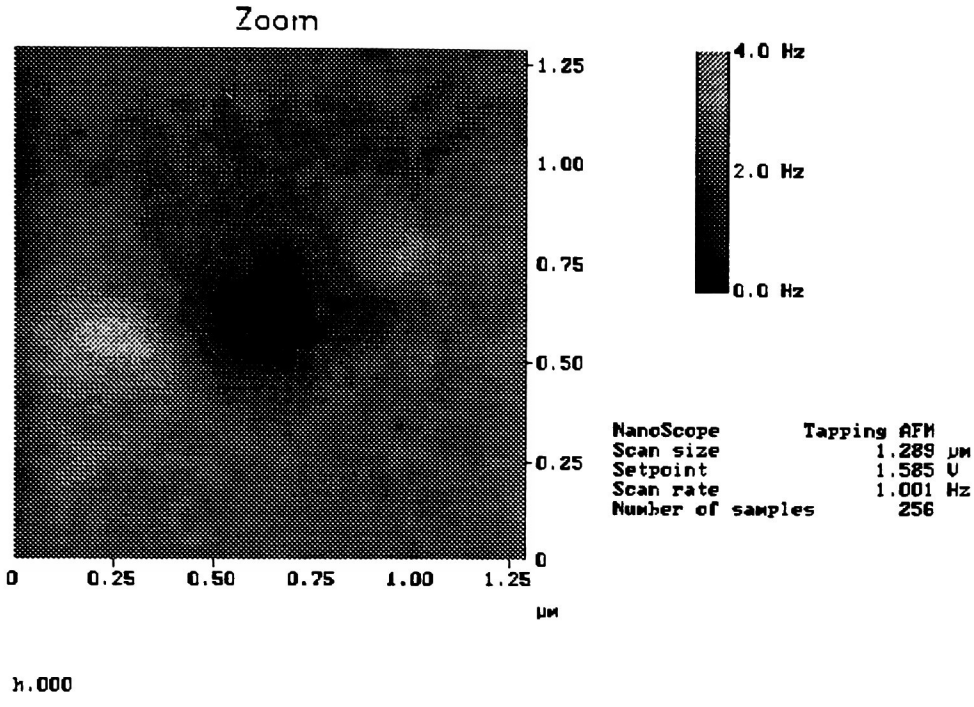

Figure 4.7. An example of a MFM image of a MD cobalt particle.

An example of a MFM image of a MD cobalt particle (not used in the analysis) is shown in Figure 4.7. Instead of having one light and one dark region characteristic of SD particles, there are a total of three regions. This indicates the presence of two magnetic domains in this particle.

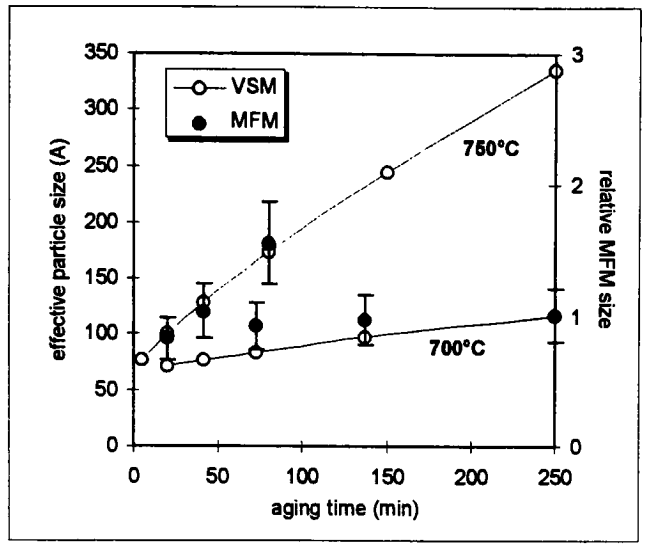

Figure 4.8. Results of MFM analysis on cobalt precipitates in Cu-Co alloys compared to results obtained using VSM analysis.

In Figure 4.8, we show the results of the MFM size analysis super-imposed on the results of the VSM size analysis. The MFM size results are scaled to show the best fit for viewing purposes. However, the actual scaling factor does not matter, since the results only yield relative sizes.

4.2. Phase analysis using x-ray diffraction

A novel method for characterizing the crystalline nature of the aged Cu-Co alloys is x-ray diffraction. We used x-ray diffraction to obtain a characteristic pattern, from which the lattice parameter of the material can be calculated as in Chapter 2.

In Figure 4.9, we show the dependence of the lattice parameter on aging time and temperature. Notice the lattice parameter for pellets aged at 700C is generally higher, indicating less cobalt in solid solution as compared to pellets aged at 750C.

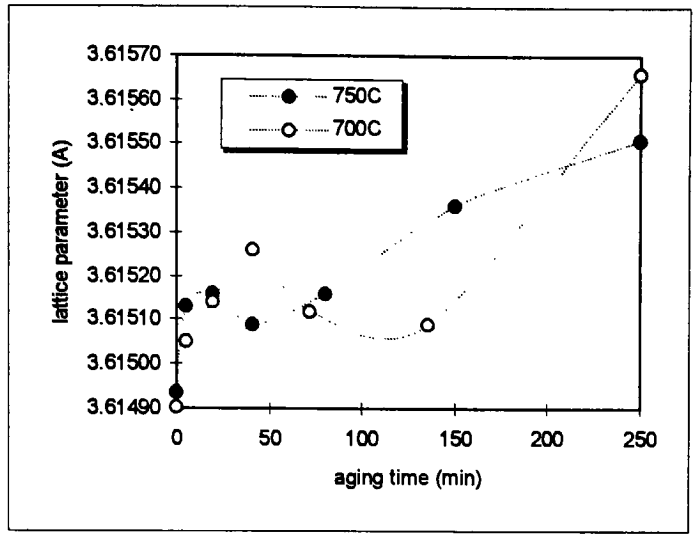

Figure 4.9. Lattice parameter of pellets aged for various times at 700C and 750C.

Recall that we previously measured a calibration curve that relates the lattice parameter of the pellets to cobalt concentration. We may use this calibration in the region from 0 to 2% cobalt to determine how much cobalt has precipitated out of solid solution for each pellet. We find the linear size factor in this region to be -0.997%.

Using this method, we show the final results of the XRD analysis along with the VSM results in Figures 4.10 and 4.11. Notice there is an unexpected decrease in the amount of cobalt precipitated out of solution indicated by XRD analysis. This decrease happens at both temperatures and near a magnetic phase transition (paramagnetic to ferromagnetic).

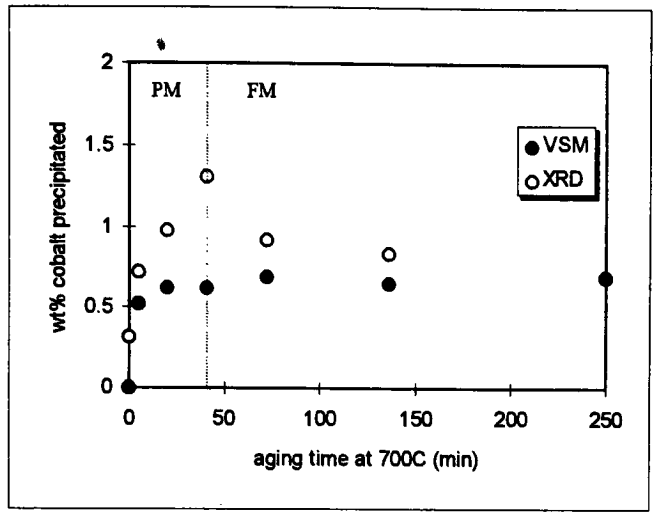

Figure 4.10. Comparison between XRD and VSM methods of determining the amount of cobalt precipitated out of solid solution as a function of aging time at 700C. We indicate the regions for which the material behaved as a paramagnet (PM) and ferromagnet (FM).

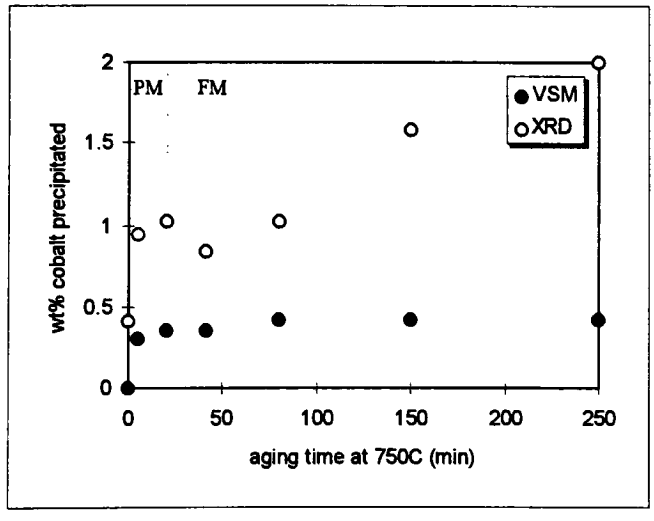

Figure 4.11. Comparison between XRD and VSM methods of determining the amount of cobalt precipitated out of solid solution as a function of aging time at 750C. We indicate the regions for which the material behaved as a paramagnet (PM) and ferromagnet (FM).

We observe an unexpected period of decreasing cobalt content for some of the pellets at both temperatures. However, there is qualitative agreement between the VSM and XRD results at both temperatures.

4.3. Discussion of aged Cu-Co alloys

XRD and VSM measurements were used to determine the amount of cobalt precipitated out of solid solution as a function of aging time and temperature. The VSM results were conclusive and corresponded well to the limits predicted by the Cu-Co alloy phase diagram solvus line.

The XRD results showed a general agreement with VSM results. However, there was a consistent decrease in lattice parameter for a certain period of the aging process. The nature of the irregularity is consistent between the two aging temperatures studied.

This phenomena may be due to the random +/- 0.00017A uncertainty associated with each measurement. This would lead us to believe that the identical trend found at both aging temperatures is coincidental.

Another explanation for the irregularity is that there may be some actual physical phenomena causing it. This is possible because the region where the decrease in lattice

parameter begins is approximately where the paramagnetic to ferromagnetic transition occurs.

We also find the temporary decrease to occur at smaller times for the higher of the two temperatures. This is characteristic of a real physical phenomena because of a higher diffusion rate of cobalt in copper at higher temperatures.

We also used VSM measurements, namely coercivity, to determine an effective particle size. In order to use this model, we also needed to develop a second model to relate particle size to aging time and temperature. The results of this analysis appear to be valid and conclusive. The particle growth is much quicker at 750C as compared to the growth at 700C. The fitted rate constants for each temperature, for which we provided a simple physical explanation, also followed well with what was expected.

MFM size analysis was used to validate the VSM size analysis. As shown in Figure 4.8, there is a good agreement between both methods. The VSM method makes more assumptions and carries more "fudge-factors". However, the MFM analysis was carried out on a particle by particle basis. This creates a lot of statistical error due to the low number of particles actually examined. Because neither method is purely quantitative and we cannot be certain of the actual magnitude of the sizes.

Chapter 5. Conclusions

5.1. Materials properties of Cu-Co alloys

We have shown that one can easily create copper-cobalt solid solutions in the bulk form. Although the solid solubility of cobalt in copper exceeds 4% at high temperatures, we were only able to prepare single phase solid solutions with 2% or less cobalt. Magnetic and x-ray diffraction measurements confirmed the presence of these complete solid solutions.

The pellets that were single phase solid solutions behaved paramagnetically. This is in contrast to bulk copper which is diamagnetic and bulk cobalt which is ferromagnetic. The paramagnetic behavior comes from the isolated cobalt atoms. As the cobalt concentration is increased, the cobalt atoms are closer and there is more of an interaction between them. We have found the initial susceptibility of the solid solutions to be proportional to the cobalt concentration squared, as expected.

After a subsequent anneal at lower temperatures, the Co precipitated out of solution and formed particles ranging from 0-300A in size. This particle size was controlled by varying the aging time and temperature. Magnetic measurements suggest a wide size distribution.

These nanometer sized cobalt particles possess special properties that cobalt does not normally have in the bulk form. Namely, the nanometer sized cobalt particles have a

fcc crystal structure at room temperature. Normally, cobalt is hcp at room temperature.

These nanometer sized cobalt particles also have a large coercivity compared to bulk cobalt. The coercivity of pellets aged at 750C peaked at 300 Oe. For the aging times studied, the pellets aged at 700C continually increased to a value of 250 Oe. These values are high for a cubic material.

This materials system serves as an ideal candidate for studying many interesting areas in materials science. First, one has many different ways to characterize and begin to further understand the nature of solid solutions. This system also provides a simple method of preparing nanometer sized magnetic particles. With the miniaturization of digital storage technologies, many researchers have interest in this area.

5.2. Success of models and characterization methods

In this project, we developed a simple minded model to understand the time it would take to put a dilute amount of cobalt into solid solution. The binary Cu-Co phase diagram phase does indicate that solid solutions are possible, but does not inform us as to how long it takes to attain one. Our solution-anneal model is important if one wishes to develop a process which prepares Cu-Co solid solutions in the smallest amount of time. After deciding on a time to solution-anneal, we used x-ray diffraction and magnetic methods to determine if a complete solid solution was created.

Once we confirmed a complete Cu-Co solid solution existed, we were able to relate the materials lattice parameter to the cobalt content successfully. Our results differ slightly from those predicted in the literature.

X-ray diffraction was effectively used in many different ways in this project. We found the repeatability of measuring a specific pellets lattice parameter to be +/- 0.00005A. In addition, we also found the repeatability of the lattice parameter of a different pellet prepared under the same conditions to be +/- 0.00017A.

From the pellet's magnetic coercivity, we were able to develop a simple model that determined an "effective" cobalt particle size. In this model, we assumed a simple power-law type relationship between particle size and aging time and temperature. From the limited amount of data obtained, our model was successful.

In the course of fitting the coercivity data to time and temperature, we had to develop another model to relate an "effective" particle size to aging time and temperature. This model worked very well. We were able to relate the growth rate to the diffusivity and solvus concentration at each temperature.

The results of the coercivity model were validated by the results of another magnetic model. We developed a **new** mathematical model for analyzing single-domain magnetic spheres using magnetic force microscopy. This model was tested by imaging

the same spheres at many different heights. In general, the results showed a 1:2 correlation between the actual lift height and the modeled lift height. In addition, we also extended the model to include an extra MFM tip magnetization component. The results of this test proved that we **can** assume the magnetization of the MFM tip is mostly in the z direction.

To understand the validity of both size models, let us summarize the assumptions made in each.

VSM size model	MFM size model
• narrow size distribution • all particles are spherical • particles are non-interacting	• particles act as magnetic dipoles • all particles are spherical • particles are non-interacting

Table 5.1. Assumptions made in VSM and MFM models.

The first assumption made by the VSM size model is that the cobalt particle size distribution is narrow. Our experimental results actually indicate a wide size distribution of particles. Next, we assume the cobalt particles are spherical. This appears to be valid due to the good correlation between the MFM image of each particle and our MFM model. Since we only consider single-domain particles for the MFM analysis, it is valid to assume that they act as dipoles. Lastly, we have assumed that the particles are non-interacting. This is assumption is validated by looking at MFM images of each pellet. They show a rather large spacing between individual particles.

Although the results of the coercivity-size model appear to be conclusive, the MFM modeling may still be the stronger of the two. The results of the VSM model provide an "effective" cobalt particle size, which is the result of some sort of averaging of the whole pellet. However, the MFM model allows one to measure the relative sizes of individual particles. This gives us a more conventional approach to particle size analysis. What was needed for better MFM results in this paper was more time to analyze many more particles and perform a thorough statistical study.

Chapter 6. Suggestions for Future Development

Although the general ideas of this project were simple, there are many areas which deserve further attention in the future.

Electrical resistivity measurements of the aged Cu-Co pellets should be made in the presence of an applied magnetic field. There is a good chance that a large magnetoresistive (MR) effect may be found. Published studies show a large MR effect in granular Cu-Co alloys. This phenomena is of particular interest to those working in the field of magnetic recording heads.

These alloys also need a more in depth MFM analysis. Due to time restrictions, only a few MFM images were taken of each pellet. If one was able to image many different areas of the same pellet, more individual cobalt particles could be analyzed. Overall, this would yield a more statistically accurate magnetic description of the cobalt particles in each pellet.

In addition, it would also be interesting to obtain MFM images in the presence of an applied magnetic field. This would allow one to study the switching behavior of the cobalt particles. In a sense, it is just like running a hysteresis loop on individual cobalt particles.

Another avenue that would be worthwhile pursuing would be to try and calibrate the MFM size analysis to yield quantitative size information. This could be done by developing a calibration standard consisting of magnetic particles of known size.

Alternate fabrication techniques could also be employed in the future. High energy ball milling (mechanical alloying) of the initial Cu-Co powders may yield new and interesting materials. In the initial stages of this project, a small amount of time was devoted to exploring this technique. Even though early results were discouraging, additional effort in this direction may generate an interesting alloy system. Other fabrication techniques include wet chemical precipitation of nanocrystalline Cu-Co powders. This has been done by some in the literature. However, if one used the analysis techniques in this project on these new nanocrystalline powders, there may be some new and interesting results to report.

Lastly, more study is needed on the crystalline properties of solid solution and aged Cu-Co materials. There appear to be some interesting phenomena taking place, that one cannot explain with the limited data obtained so far. For example, we may attempt to explain whether or not there is actually a local minimum in Figures 4.10 and 4.11. This may be an indication that there is something happening during the paramagnetic to ferromagnetic transition.

Appendix 1. Summary of magnetic terms used in this project

coercivity	reverse magnetic field required to make the magnetization of a material zero, which is also a measure of how easy or hard it is to read/write information on magnetic storage disks
ferromagnet	magnetic state of a material in which there is a measurable coercivity and large magnetic moment
hysteresis loop	plot which shows the moment of a magnetic material as a function of applied magnetic field
magnetic moment	measure of how "magnetic" a material is
remanent magnetization	measure of how magnetic a material is in the absence of an applied magnetic field
paramagnet	magnetic state of a material in which there is no coercivity and a small magnetic moment which is not easily saturated
superparamagnet	magnetic state of a material in which there is no coercivity and large magnetic moment which is easily saturated
saturation magnetization	measure of how magnetic a material is in the presence of a very large magnetic field, which is usually representative of how much magnetic material is present

Appendix 2. Alphabetical listing of references

T. R. Albrecht et al, Frequency modulation detection using high-Q cantilevers for enhanced force microscopy sensitivity, J. Appl. Phys. **69** (2), p668, 1991.

ASM Metals handbook, Volume 3: Alloy Phase Diagrams, ASM International, 1991.

J. J. Becker, Magnetic method for the measurement of precipitate particle sizes in a Cu-Co alloy, Trans. AIME, p59, Jan 1957.

J. J. Becker, Precipitation and magnetic annealing in a Cu-Co alloy, Trans. AIME, p139, Feb 1958.

J. J. Becker, J. D. Livingston, A study of precipitation-hardening employing magnetic measurements, Trans. AIME, p316, June 1958.

A. E. Berkowitz et al, Giant magnetoresistance in heterogeneous Cu-Co alloys, Phys. Rev. Lett., **68** (25), p3745, 1992.

M. Breu, W. Gust, B. Predel, Influence of doping on the early stages of precipitation in Cu-Co-base alloys, Mat. Sci. Eng., **A151**, p61, 1992.

J. G. Cabana-Moreno et al, Mechanical alloying of Co-Cu powder mixtures, Scr. Meta. et Mat., **28**, p645, 1993.

J. R. Childress, C. L. Chien, Reentrant magntic behavior in fcc Cu-Co alloys, Phys. Rev. B, **43** (10), p8089, 1991.

G. M. Chow et al, Structural, morphological, and magnetic study of nanocrystalline cobalt-copper powders synthesized by the polyol process, J. Mat. Res., **10** (6), p1546, 1995.

B. D. Cullity, Introduction to Magnetic Materials, Addison-Wesley, 1992.

R. Dohl et al, Measurement of the diffusion coefficient of cobalt in copper, Phys. Stat. Sol. A, **86**, p603, 1984

S. Foner, Versatile and sensitive Vibrating Sample Magnetometer, Rev. Sci. Instr., **40** (7), 1959.

S. Gangopadhyay et al, Magnetic properties of ultrafine Co particles, IEEE Trans. Mag., **28** (5), p3174, 1992.

C. Gente, M. Oehring, R. Bormann, Formation of thermodynamically unstable solid solutions in the Cu-Co system by mechanical alloying, Phys. Rev. B, **48** (18), p13244, 1993.

S. K. Gupta, B. D. Cullity, Problems associated with K doublet in residual stress measurements, Advances in X-Ray Analysis, **23**, p333, 1980.

V. G. Harris et al, Structure and magnetism of heat-treated nanocrystalline $Cu_{80}Co_{20}$ powders prepared via chemical means, J. Appl. Phys, **75** (10), p6610, 1994.

Jade v3.0 Data Aquisition software.

S. Kalpakjian, Manufacturing Engineering and Technology, Addison-Wesley, p505.

D. Rugar et al, Magnetic force microscopy: General principles and application to longitudinal recording media, J. Appl. Phys.,**68** (3), p1169, 1990

D. Saird, Scanning Force Microscopy, Oxford University Press, p158, 1991.

I. S. Servi, D. Turnbull, Thermodynamics and kinetics of precipitation in the Copper-Cobalt system, Acta. Meta., **14**, p161, 1966.

W. F. Smith, Materials Science and Engineering, 2nd Ed., McGraw-Hill, p162, 1990.

R. Tournier, A. Blandin, Influence of interactions between impurities on the appearance of magnetic moments in Cu-Co dilute alloys, Phys. Rev. Lett. **24** (8), p397, 1970.

J. Q. Xiao, J. S. Jiang, C. L. Chien, Giant magnetoresistance in nonmultilayer magnetic systems, Phys. Rev. Lett., **68** (25), p3749, 1992.

Y. Yoo, S. Yu, W. Kim, Magnetic properties of nanocrystalline Cu-Fe-Co alloys processed by mechanical alloying, IEEE Trans. Mag., **31** (6), p3769, 1995.

R. H. Yu et al, Magnetic properties and giant magnetoresistance in magnetic granular Co_xCu_{100-x} alloys, J. Phys. D: Appl. Phys. **28**, p1770, 1995.